In Situ Measurement of pH and Dissolved H_2 in Mid-Ocean Ridge Hydrothermal Fluids at Elevated Temperatures and Pressures

Kang Ding* and William E. Seyfried, Jr.

Department of Geology and Geophysics, University of Minnesota, 310 Pillsbury Drive E, Minneapolis, Minnesota 55455

Received April 20, 2006

Contents

1. Introduction 601
2. In Situ pH Sensor 602
   2.1. Theoretical Considerations of Sensor Design 603
      2.1.1. Thermodynamic Constraints 603
      2.1.2. Sensor Construction and Testing 603
   2.2. Experimental Verification 604
      2.2.1. Preliminary Response Characteristics 604
      2.2.2. Correspondence with the Standard Hydrogen Electrode 605
      2.2.3. Theoretical Response and Assessment 605
3. Dissolved H_2 Sensor 606
   3.1. Sensor Design and Construction 607
   3.2. Verification of Sensor Performance 607
      3.2.1. Temperature Constraints on Sensor Response 607
      3.2.2. Reversibility 608
      3.2.3. Nernstian Response 608
4. In Situ Measurements at Seafloor Hydrothermal Vents 609
   4.1. Sensor Unit Design for the Seafloor Deployment 610
      4.1.1. Mechanical Considerations 610
      4.1.2. Electronics and Data Communication 611
   4.2. In Situ pH Measurement 612
      4.2.1. Sensor Response 612
      4.2.2. Uncertainties with the In Situ pH Value 612
      4.2.3. Verification of the Vent fluid $pH_{(in-situ)}$ 613
   4.3. In Situ Dissolved H_2 Measurements 614
      4.3.1. Field Verification 614
      4.3.2. Steady-State Measurements 615
      4.3.3. Dynamic Scan Mode 616
      4.3.4. Time Series Monitoring 617
5. Future Prospects 618
   5.1. Long-term Stability of YSZ Ceramic in Hydrothermal Fluids 619
   5.2. Reference Electrode for pH Measurement 619
6. Conclusions 620
7. Acknowledgements 621
8. References 621

1. Introduction

Ever since the discovery in 1979 of high-temperature hydrothermal fluids issuing from chimney structures at 21° N East Pacific Rise (EPR), the need was clear for in situ data to constrain better the chemical and temporal evolution of the system.[1−9] The combination of elevated temperatures

* To whom correspondence should be addressed. Tel.: (612) 626-1860. Fax: (612) 625-3819. E-mail: mlcd@umn.edu.

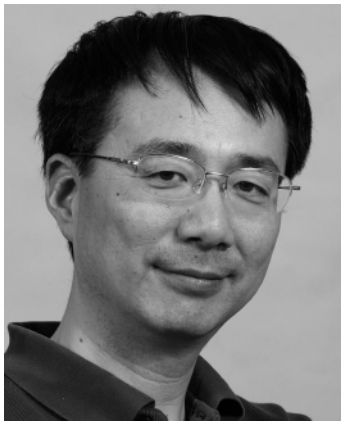

Kang Ding received his Ph.D. degree in geochemistry in 1987 at Institute of Geochemistry, Chinese Academy of Science, under the supervision of Dr. Guangzhi Tu. He is currently a senior research associate in University of Minnesota. His field of research involves hydrothermal chemistry with an emphasis on subseafloor systems. These studies are mainly carried out through experimental effort at elevated temperatures and pressures, especially in the supercritical region of water. In past 10 years, he has been involved extensively with deep submergence science for developing and applying in situ chemical sensors to study hydrothermal fluids venting at mid-ocean ridges.

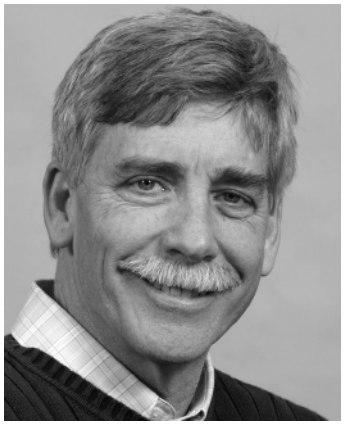

William E. Seyfried, Jr., obtained his Ph.D. degree in geology from the University of Southern California in 1977. Presently, he is Professor of Geochemistry at University of Minnesota, a position he has held since 1987. From 1993 to 2006, he served as the chairman of the Department of Geology and Geophysics and Head, Newton Horace Winchell School of Earth Sciences, at the University of Minnesota. At present, he is involved in experimental, field, and theoretically based studies related to hydrothermal processes at a wide range of temperatures and pressures with application specifically to mid-ocean ridge hydrothermal systems.

10.1021/cr050367s CCC: $65.00
Published on Web 01/20/2007

and pressures with the complex mixing processes between seawater and end-member vent fluid underscored the challenging nature of the task. These challenges notwithstanding, laboratory efforts were soon launched to test and develop electrochemical approaches that could be used to constrain the most critical components of the vent fluids. For virtually all of geochemical systems, pH and redox (e.g., dissolved H_2) are typically considered master variables in that these variables control the direction and magnitude of mass transfer reactions and the formation of secondary alteration minerals. Conventional approaches used to indirectly constrain the activities of these species most often relied on fluid sampling and subsequent analysis, followed by application of a series of algorithms to correct the lab-measured chemical data for the effects of cooling and decompression.[1,3−6,10−12] Although success for some species has been achieved through this approach, uncertainties for others are large. For instance, apart from cooling-induced precipitation of metal sulfides and oxides, which clearly influence the measured pH ($pH_{(25°C)}$) of the quenched vent fluid sample, simultaneous dissociation of H^+- and OH^--bearing aqueous complexes and ion pairs contributes further to the complicated process of reconstructing the pH of the fluid at elevated temperatures and pressures ($pH_{(in-situ)}$) from ship-board measurements. In general, the role of the temperature- and pressure-induced changes in speciation on pH can be described as follows:

$$mH^+_{25°C} = \sum mHX^\circ_{T,P} + mH^+_{T,P} - \sum mYOH^\circ_{T,P} \quad (1)$$

where HX° and YOH° represent idealized acids and bases, respectively, the stabilities of which are explicit functions of temperature, pressure, and fluid composition. Thus, the concentration of free H^+ in the quenched fluid ($mH^+_{25°C}$) is clearly not the same as that at high temperature and pressure ($mH^+_{T,P}$). This is especially true for hydrothermal fluids near the critical point of seawater (408 °C) where H^+-bearing aqueous complexes are strongly associated but which can be rendered unstable with slight chemical and physical change.[13,14] Thus, the challenge of determining in situ pH of a chemically complex vent-fluid from measured $pH_{(25°C)}$ data involves the need to explicitly account not only for the full chemistry but also the temperature and pressure dependent changes in the distribution of aqueous species. This indirect approach is often limited by the availability of the related thermodynamic data.

Besides the uncertainties related to temperature- and pressure-dependent speciation effects on determining $pH_{(in-situ)}$, the likelihood of entraining seawater with vent fluid while sampling changes the bulk fluid chemistry complicating further the reconstruction of in situ chemical data from that regressed from quenched vent fluid samples. Although we have emphasized the effect of this on pH, somewhat similar processes apply to highly reactive dissolved gas components, such as H_2.

Because of mixing-induced mineral precipitation and cooling effects on pH and dissolved H_2, the attention that has been focused on in situ measurement approaches is not surprising. However, any in situ approach faces severe technological and theoretical constrains owing to the extreme chemical and physical conditions characterizing seafloor hydrothermal vent fluids. Perhaps the most difficult obstacle to overcome is the relative lack of chemically and mechanically stable materials that can serve as chemical sensors in the high temperature acidic chloride- and sulfide-bearing vent fluid. At temperatures above 350 °C, few materials have the unique characteristics of chemical stability and electrochemical properties favorable for sensor development, although some ceramic-based phases and precious metals satisfy both attributes. A second factor that needs to be addressed involves the routine availability of basic thermodynamic data applicable to compositionally complex aqueous fluids at elevated temperatures and pressures. Under these conditions, and especially when chemical and physical conditions approach the supercritical region, ionic association becomes highly nonlinear with small changes in temperature or pressure, placing severe constraints on the required accuracy of the thermodynamic database.[13] In the case of $pH_{(in-situ)}$ measurements, thermodynamic data for H^+- and Cl^--bearing species at the corresponding conditions must be available so that the total measured Cl can be accurately converted to the individual ion activity. Additionally, all sensor components involving external casings, internal signal processing, data storage, and data communication must be designed in such a way to sustain the operation in extreme environments.

In spite of these difficult challenges, knowledge of vent fluid is sufficiently important to so many geochemical and biogeochemical processes at and below the seafloor that efforts to develop successful direct measurement strategies at elevated temperatures and pressures are well justified. It is especially true for $pH_{(in-situ)}$ and dissolved H_2, as they are two of the most important and critical chemical parameters for understanding the vent system. Thus, the priority to develop in situ sensing methods for measuring and monitoring H^+ and dissolved H_2 activity/concentration are warranted. The recent advances in material science, sensor technology, and experimental and theoretical high-temperature solution chemistry have also made it possible to develop in situ chemical sensors for carrying out measurement and monitoring tasks under extremely challenging conditions at the seafloor hydrothermal vents. In this communication, we will review the recent development on high-temperature in situ pH and dissolved H_2 measurements, which is related and has been applied to the study of mid-ocean ridge hydrothermal system. Although a great amount of the work has been done regarding in situ chemical measurement in hydrothermal systems, it is mostly designed to address laboratory or industrial applications as reviewed recently by Lvov and Palmer[15] and Zhu et al. [16] The effort aimed at high-temperature seafloor hydrothermal vent fluids is still in its early stage and is very limited. In the following, we will focus our treatment of seafloor high-temperature in situ pH and dissolved H_2 sensors on theoretical and laboratory/field verification methods. These verification studies lend confidence to measurements with chemical sensors at vent to constrain better subseafloor hydrothermal alteration processes.

2. In Situ pH Sensor

Numerous efforts have been made to develop chemical sensors for pH measurement in hydrothermal fluids. In relatively low-temperature vent fluid systems, glass electrodes are still candidates for making pH measurements. For example, Le Bris et al.[17,18] has successfully conducted direct pH measurements in a seafloor hydrothermal diffuse flow environment with a combination glass−Ag/AgCl electrode at temperatures as high as 120 °C and pressures equivalent to ocean depths of 2600 m. In this case, conventional pH buffers were used as calibration standards. The accuracy of

these measurements is reported to be <0.2 and 0.5 pH units, respectively, for temperatures less than and greater than 75 °C.[18] At high-temperature conditions, hydrogen concentration cells,[19−23] as well as palladium hydride electrodes,[24] have been used successfully to determine pH at subcritical temperatures (<320 °C) and relatively low pressures (<250 bar). Yittria-stabilized zirconia (ZrO_2 ($9\%Y_2O_3$)) ceramic membrane electrodes (YSZ),[25−27] however, have provided better alternatives for measuring pH at relatively high temperatures (>150 °C), especially in the supercritical region of water.[28−33] At present, YSZ is the only material with sufficient chemical stability and appropriate electrochemical properties for measuring pH directly in fluids at temperatures at or above the critical point of water. It is also the most effective means of measuring in situ pH directly in NaCl-dominated hot spring fluid at temperatures and pressures applicable to mid-ocean ridge hydrothermal systems.[32,34] Besides the obvious difficulties imposed by temperature, the reality of in situ pH measurements is also confronted by the lack of direct approaches to verify the accuracy of pH measurement in aqueous fluids at elevated temperatures and pressures; that is, unlike pH determination at temperatures less than 100 °C where pH buffers exist, the same is not true at the extreme conditions typical of subseafloor hydrothermal fluids. Thus, alternative verification techniques are necessary to provide the same level of confidence in pH measurement as exists at low temperatures and pressures. The operational mechanism and thermodynamic basis of YSZ for pH measurement has been extensively discussed and reviewed.[27,33] Thus, we will focus our attention here on design and verification methods supporting the use of YSZ membrane electrodes to constrain the chemistry of seafloor hydrothermal vent fluids.

2.1 Theoretical Considerations of Sensor Design

Ever since the first discovery of the pH-sensing characteristics of YSZ ceramic at temperatures as high as 300 °C in the early 1980s, much attention has been focused on extending its application to a higher temperature range, especially into the supercritical range of water.[27−33] The first attempt in 1992 to use YSZ solid-state electrodes at supercritical aqueous conditions proved successful by yielding pH data for low ionic strength fluids.[28] Since YSZ ceramic has negligible electronic conductivity at temperature conditions less than 450 °C, it is insensitive to the changes in redox.[25−27,35] Moreover, laboratory studies have demonstrated that it is highly corrosion resistant, in either acidic or basic fluids, as well as in concentrated NaCl fluids, at a wide range of temperatures and pressures.[28,32,36] Studies have also demonstrated that the pH response of the YSZ sensor is unaffected by elevated concentrations of dissolved sulfide, an attribute essential for application involving subseafloor hydrothermal fluids.[27]

2.1.1 Thermodynamic Constraints

YSZ ceramic provides an unparalleled material allowing measurements (Emf) specific to the activity of H^+ ion in coexisting fluid.[27] When coupled with the Hg/HgO internal reference electrode that can be enclosed within YSZ tubing, the following relationship results:

$$E_{YSZ} = E^\circ_{Hg/HgO} - \frac{2.303RT}{2F}\log(a_{H_2O}) - \frac{2.303RT}{F}\,pH \quad (2)$$

where R, F, and T stand for the gas constant, Faraday constant, and temperature (K), respectively, while a_{H_2O} is the activity of water, and $E^\circ_{Hg/HgO}$ is the standard potential for the Hg/HgO internal reference element, which can be defined as follows:

$$HgO + 2H^+ + 2e^- \leftrightarrow Hg + H_2O \quad (3)$$

Accordingly, with a suitable reference electrode, such as Ag/AgCl, an electrochemical cell for pH measurement can be derived:

$$Ag \mid AgCl \mid Cl^-, H^+, H_2O \mid YSZ \mid Hg \mid HgO \quad (4)$$

The overall cell potential for eq 4 at a specific temperature and pressure ($\Delta E(V)_{TP}$) is as follows:

$$\Delta E(V)_{T,P} = \Delta E(V)^\circ_{T,P} - \frac{2.303RT}{F}\left[\log a(Cl^-) - \frac{1}{2}\log(a_{H_2O}) - pH_{(in-situ)}\right] \quad (5)$$

where $\Delta E(V)^\circ_{T,P}$ is the standard cell potential at the appropriate temperatures and pressures as determined from standard state potentials of $E_{Ag/AgCl}(V)^\circ_{T,P}$ and $E_{Hg/HgO}(V)^\circ_{T,P}$, while $a(Cl^-)$is the activity of dissolved chloride. From this relationship, it is clear that changes in fluid pH will result in corresponding changes in the overall cell potential (Emf). For instance, at 400 °C, one unit change in pH will result in a change of 0.134 V ($\Delta E(V)_{TP}$), which is consistent with the Nernst slope defined by eq 5. Thus, $pH_{(in-situ)}$ of a fluid at an elevated temperature and pressure can be determined through the measurement of a DC signal ($\Delta E(V)_{TP}$):

$$pH_{(in-situ)} = \frac{F}{2.303RT}[\Delta E(V)_{T,P} - \Delta E(V)^\circ_{T,P}] + \left[\log a(Cl^-) - \frac{1}{2}\log(a_{H_2O})\right] \quad (6)$$

Activity of dissolved chloride can be determined from the measured total chloride concentration taking explicit account of the distribution of aqueous species and the activity coefficients of the aqueous species using thermodynamic data at the appropriate temperature and pressure conditions.[37−47]

2.1.2. Sensor Construction and Testing

The YSZ membrane electrode described here was modified after procedures developed by Macdonald et al.[29] In particular, a YSZ tube made by Coors Ceramics Co. was chosen as the sensing body (Figure 1). The ceramic tube is 0.625 cm in diameter, 0.475 cm in wall thickness, and 7.5 cm in length. Native Hg and synthetic HgO (99.998% pure from AESAR) were combined and placed inside the tube at its base. A Pt wire connected to the Hg/HgO paste served as a conductor and facilitated electrode response. The YSZ tube was then filled to the top with high-temperature ceramic epoxy (SiO_2 base from Cotronics Corp.). For testing, the YSZ ceramic membrane electrode was then installed into a high-pressure flow reactor constructed using a Teflon sealant and Conax fitting (Conax Buffalo, NY).[30]

Considering the highly corrosive fluids that would be used to test YSZ sensor response, the flow-reactor (50 mL volume) was constructed entirely of titanium and titanium alloy (6Al4V). The flow-reactor was designed in such a way that both the YSZ sensor and the associated reference electrode could be secured sufficiently to sustain temperatures and

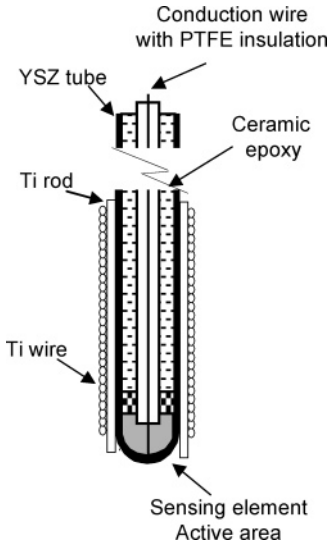

Figure 1. Schematic diagram showing the YSZ−pH electrode. The Ti wire external to the electrode inhibits cracking of the ceramic due to thermal shock in the high-temperature vent fluids.

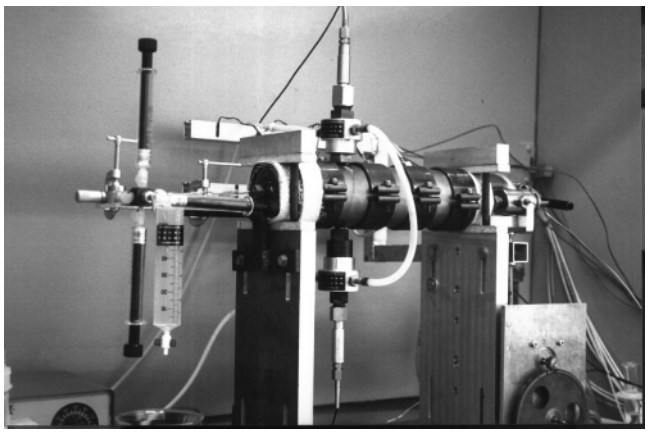

Figure 2. Ti-flow reactor designed to permit development and testing of in situ sensors in aqueous fluids at supercritical conditions. Fluid samples can be taken at experimental conditions through a Ti sampling valve, providing an additional constraint on the validity of sensor measurements and performance.

pressures as high as 425 °C and 500 bar (Figure 2), which are needed to simulate conditions in subseafloor reaction zones at mid-ocean ridges.[30] Fluid flowing through the reactor could be maintained at rates from 0.1 to 8.0 mL/min using an HPLC pump, which is also constructed of titanium. A computer-controlled titanium-metering valve regulated pressure. Fluid samples could be collected at experimental conditions by opening a titanium-sampling valve and allowing fluid to enter a sample loop or gastight syringe. Simultaneously, replacement fluid is delivered to the reactor by the HPLC pump, maintaining pressure and flow rate constant. A set of band heaters (Watlow-Gordon) was used to maintain temperature at a constant value (±0.5 °C). A band heater was also used to preheat fluid entering the reactor. Each band heater can be independently controlled and monitored to ensure maximum thermal stability over the entire length of the flow reactor.

In operational mode, the periodic removal of fluid samples from the flow-reactor allowed monitoring of fluid chemistry. Accordingly, fluid samples were analyzed for Cl, Na, and $pH_{(25°C)}$, as well as trace elements (Zr, Y, Ca, Al, Si, transition metals), which, when present, likely were derived from sensor or reactor components. Inductively coupled plasma−mass spectrometer (ICP−MS) or ion chromatograph (IC) was utilized for all measurements of dissolved species, other than $pH_{(25°C)}$, which was measured using a Ross-type glass electrode (ORION) with calibration standards (Fisher Scientific) that buffered pH at 2.00, 4.00, 7.00, and 10.00. Results reveal that the sensor and reactor components were stable under experimental conditions, as evidenced by contaminant concentrations that did not exceed 10^{-4} mol/kg, even for input fluids having $pH_{(25°C)}$ as low as 1.91 (Table 1). As the fluid with variable pH flowed into the reactor,

Table 1. Dissolved Chemistry of Fluids Coexisting with YSZ and 0.55 mol/kg NaCl in Ti Flow Reactor at 400 bar[a]

run no.	M1	M2	M3	M4	M5
T °C	400	400	400	350	300
$pH_{(25°C)}$	1.91	2.96	4.60	1.86	1.86
Al	9.5	1.04	0.15	0.22	1.52
Si	97.9	21.7	19.2	97.1	94.9
Ca	50.1	7.39	11.5	40.0	43.2
K	7.03	18.0	16.9	8.77	1.17
Mg	3.79	1.44	5.59	3.87	3.54
Sr	0.37	0.32	0.26	0.33	0.33
Y	20.0	0.24	0.01	17.2	12.9
Zr	0.03	0.05	0.04	0.03	0.03
Ti	1.34	0.13	0.10	1.29	1.23
Cr	0.48	0.46	2.17	1.77	4.29
Fe	31.4	21.2	1.24	28.9	30.7
Mn	0.84	0.27	0.27	0.86	0.96
Ni	7.22	2.71	1.60	5.61	6.41
Cu	0.63	0.46	0.13	0.24	0.39
SO_4^{2-}	11.50		15.09		

[a] Unit for concentration: μmol/kg. Flow rate: 2 mL/min.

cell potential was measured with a Keithley 2001 or 6517 electrometer with an input impedance of 1×10^{11} to $1 \times 10^{14}\Omega$. Uncertainties in the measurements were thus generally within ± 0.003 V at 95% confidence level.

2.2. Experimental Verification

The above theoretical relationships (eqs 2, 5, and 6) clearly indicate that the YSZ−pH sensor is a thermodynamic or primary electrode and is not empirically based,[27] a distinction that is very significant. Thus, the YSZ sensor does not require calibration in a strict sense, since the response of the sensor to pH is dictated by the thermodynamic properties of the internal reference (Hg/HgO). Accordingly, the pH−$\Delta E(V)_{TP}$ response necessarily follows Nernst law. This characteristic provides a fundamental basis for verifying the performance of the sensor. Since calibrated pH buffers do not exist at chemical and physical conditions analogous to those typical in subseafloor reaction zones at mid-ocean ridges, the most suitable method for "testing" the sensor response is by comparing the measured response to pH with that theoretically predicted. If defects or compositional variability exist in the YSZ ceramic, however, experimental verification is increasingly important. Our approach has been to assume that this is the case and then to conduct verification studies.

2.2.1. Preliminary Response Characteristics

The rate of response of the YSZ sensor to pH change in aqueous fluids at elevated temperatures and pressures can be confirmed by tests using the flow-through reactor. In effect, the pH of the source fluid can be easily and

systematically adjusted, while corresponding measurements of pH at experimental conditions ($pH_{(in-situ)}$) by the YSZ and coexisting reference electrode are simultaneously monitored. Data reveal that the in situ pH sensor responds rapidly and reversibly to pH change. For example, tests performed at 400 °C and 400 bar (Figure 3) indicate an immediate sensor

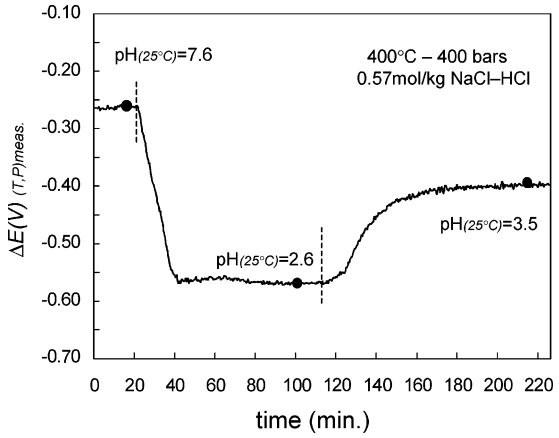

Figure 3. YSZ cell potential $\Delta E(V)_{(T,P)meas}$ vs recording time during a typical flow-through experiment with 0.57 mol/kg NaCl−HCl solution at 400 °C and 400 bar (modified after ref 32). Dash lines indicate changes in the $pH_{(25°C)}$ (7.6 to 2.6 and 2.6 to 3.5) of source fluid. Solid symbols represent real time measurements of $pH_{(25°C)}$ of fluid leaving the reactor. Taking account of reactor volume (50 mL), and flow rate (2 mL/min), which promotes continuous fluid mixing, data indicate that cell potential responds rapidly to changes in acidity of the source fluid.

response of 0.300 V when the pH of the source fluid is switched from unacidified 0.57 mol/kg NaCl solution ($pH_{(25°C)} = 7.6$) to a distinctly acid fluid ($pH_{(25°C)} = 2.6$), with the same NaCl concentration. Increasing the source fluid $pH_{(25°C)}$ to 3.5 results in an immediate corresponding increase in cell voltage.[32]

2.2.2. Correspondence with the Standard Hydrogen Electrode

The "gold-standard" for establishing the theoretical validity of pH measurements at virtually all temperatures and pressures involves comparison with data derived from the standard hydrogen electrode. Indeed, such tests were carried out early in the development of the YSZ−pH cell by Macdonald et al. and Hettiarachchi et al.[27,48]

According to the 1960 Stockholm Convention, the potential-determining equilibria for the standard hydrogen electrode is as follows:

$$2H^+ + 2e^- \leftrightarrow H_2 \tag{7}$$

where the cell potential can be more conveniently depicted as

$$E_H = -\frac{2.303RT}{2F}\log(f_{H_2}) - \frac{2.303RT}{F}\,pH \tag{8}$$

As depicted above, the measured potential is clearly a function of both H_2 fugacity and pH at a given temperature and pressure. If the YSZ pH response is identical to that of standard hydrogen electrode, then by combining eqs 8 and 2, the pH term can be eliminated, as follows:

$$\Delta E_{YH} = E_{YSZ} - E_H = \left[E^\circ_{Hg/HgO} + \frac{2.303RT}{2F}\log\left(\frac{f_{H_2}}{a_{H_2O}}\right)\right] \tag{9}$$

Thus, for a given temperature and pressure and fugacity of dissolved hydrogen (depicted here as f_{H_2}), ΔE_{YH} is a constant, which should be independent of pH. Therefore, measurements of E_H and E_{YSZ} against a common reference electrode (Ag/AgCl) ($\Delta E_{H/ref}$ and $\Delta E_{YSZ/ref}$) in fluids with different pH values should yield a line having a slope of unity:

$$\Delta E_{H/ref} = \Delta E_{YSZ/ref} - \left[E^\circ_{Hg/HgO} + \frac{2.303RT}{2F}\log\left(\frac{f_{H_2}}{a_{H_2O}}\right)\right] \tag{10}$$

This, in fact, is precisely what has been determined from numerous experimental measurements at a wide range of pH values, temperatures, and pressures (Figure 4).[27,28]

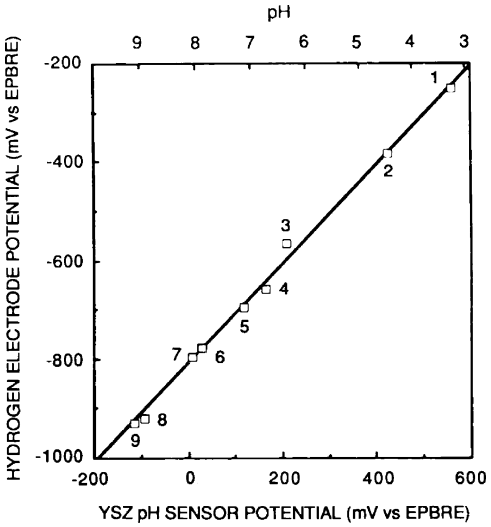

Figure 4. Correlation of standard hydrogen electrode and YSZ−pH sensor potentials at 300 °C for standard solutions: 1, 0.01 mol/kg H_3PO_4; 2, 0.1 mol/kg $NaHSO_4$; 3, 0.01 mol/kg $B(OH)_3$; 4, 0.01 mol/kg H_3PO_4 + 0.14 mol/kg NaOH; 5, 0.01 mol/kg $B(OH)_3$ + 0.0001 mol/kg KOH; 6, 1 mol/kg Na_2SO_4; 7, 0.01 mol/kg $B(OH)_3$ + 0.001 mol/kg KOH; 8, 0.01 mol/kg $B(OH)_3$ + 0.01 mol/kg KOH; 9, 0.01 mol/kg KOH. The observed correspondence between the two in situ techniques demonstrates the thermodynamic viability of YSZ pH sensor. EPBRE indicates that the potentials were measured against an external pressure-balanced reference electrode (Ag/AgCl). Reprinted with permission from ref 27. Copyright 1988 Plenum Publishing Corporation.

2.2.3. Theoretical Response and Assessment

As demonstrated above, the empirical data confirming the YSZ−pH response and comparison of this response with constraints imposed by the standard hydrogen electrode verify the functionality of the YSZ electrode for pH measurement of aqueous fluids at elevated temperatures and pressures. Verification can be extended further, however, by comparison of the electrode response characteristics with calculated in situ potential and pH data that can be determined from available thermodynamic data. Indeed, recent advances in high-temperature solution chemistry have

made it possible to predict in situ data for aqueous species in the NaCl−HCl−H_2O system at a wide range of temperatures and pressures based on available theoretical models and experimental data.[37−47]

To carry out this assessment of sensor potential ($\Delta E(V)_{(T,P)}$), the distribution of aqueous species calculated in the NaCl−HCl−H_2O system needs to be combined with mass action, mass balance, and charge balance constrains, and then compared with actual electrochemical measurements under the same chemical and physical conditions.[8] When accomplished, data reveal a good agreement between $\Delta E(V)_{(T,P)}$ and the theoretically calculated sensor potential ($\Delta E(V)_{(T,P)\text{calc}}$), even at temperatures and pressures as high as 400 °C and 400 bar, respectively (Figure 5).[32] The

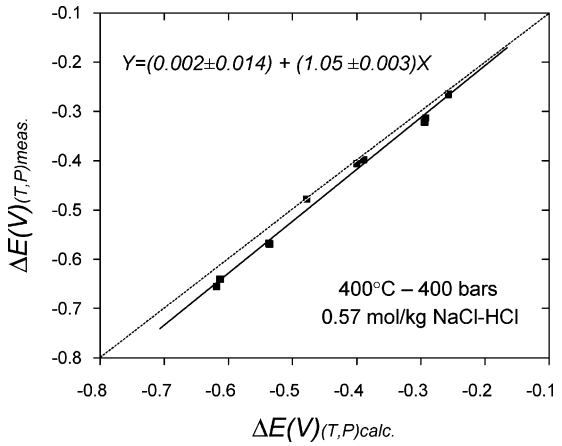

Figure 5. Measured potential $\Delta E(V)_{(T,P)\text{meas}}$ of the YSZ−pH sensor versus the theoretically predicted value $\Delta E(V)_{(T,P)\text{calc}}$ calculated for 0.57 mol/kg NaCl−HCl fluid at 400 °C and 400 bar (modified after ref 32). Results reveal a good agreement between the two independently obtained sensor potential values. In effect, the near unit slope and zero intercept of the regression line (solid line) indicate that the measured sensor response agrees well with that predicted from available thermodynamic data. Dashed line shows ideal 1:1 relation between measured and calculated values.

observed correspondence implies that the measured cell response is entirely consistent with available thermodynamic data for the system at the conditions closely related to subseafloor hydrothermal alteration processes at mid-ocean ridges.[6,8,9,49]

Another way to view the viability of the YSZ−pH response is by the slope of the line depicting changes in measured $\Delta E(V)_{(T,P)}$ with corresponding changes in $pH_{(\text{in-situ})\text{calc}}$, which can then be related to Nernst slope predictions. Using this approach, a good linear relationship is observed over the entire range of conditions investigated (Figure 6).[32] More importantly, however, within the measurement error (2σ) the slope of the regression line ($0.140 \pm 0.004(1\sigma)$) agrees with the predicted value of 0.134. As a final example, $pH_{(\text{in-situ})}$ determined from sensor measurements can be directly compared with theoretically predicted values for the full range of $pH_{(25°C)}$ investigated (Figure 7). The range of pH values investigated was designed to encompass pH values likely for mid-ocean ridge vent fluids at high temperature and pressure conditions.[6,8,9] Once again, the agreement between measured and predicted data is excellent, with the possible exception of unusually low pH conditions, where the supporting thermodynamic data or the assumptions in the calculation is less well constrained.

Taken together, these sorts of comparisons provide strong support for the theoretical foundation and general validity

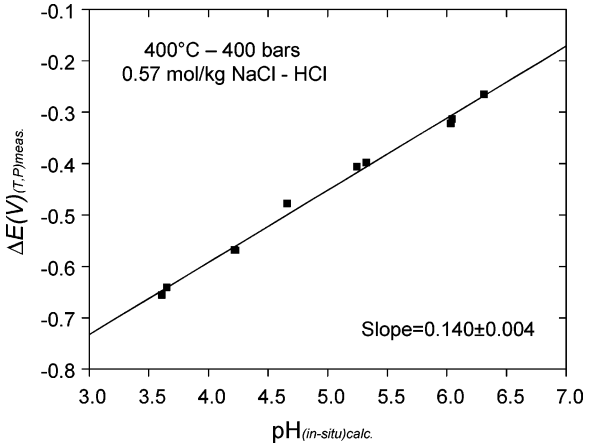

Figure 6. Measured potential $\Delta E(V)_{(T,P)}$ for YSZ−pH sensor at 400 °C and 400 bar plotted against theoretically calculated $pH_{(\text{in-situ})\text{calc}}$ to constrain the thermodynamic viability of the sensor (modified after ref 32). The slope of the linear correlation is very close to that predicted for standard Nernstian response (0.134) at the conditions tested, which suggests that the YSZ−pH sensor is thermodynamically sound and responds specifically to $pH_{(\text{in-situ})}$.

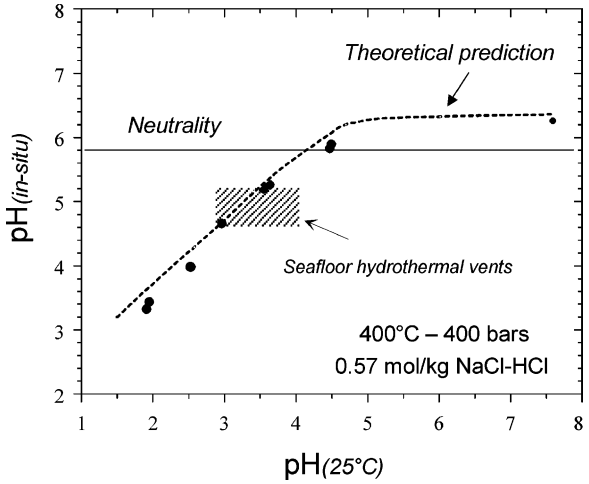

Figure 7. $pH_{(\text{in-situ})}$ as a function of $pH_{(25°C)}$ in 0.57 mol/kg NaCl−HCl solution (modified after ref 32). The direct measurements from the pH sensor confirm theoretically predicted relationship between $pH_{(25°C)}$ and pH at 400 °C and 400 bar, especially in the $pH_{(\text{in-situ})}$ range similar to seafloor hydrothermal vents fluids,[7−9] which is marked by the shaded region. Solid symbols indicate $pH_{(\text{in-situ})}$ actually measured, while the dash line indicates theoretically predicted values. Neutrality at 400 °C and 400 bar is shown for reference.

of using the YSZ sensor to measure pH of aqueous fluids at elevated temperatures and pressures. These data, together with constraints imposed by results of laboratory studies, establish a framework justifying application of the YSZ−pH senor for pH measurement and monitoring of hydrothermal vent fluids at mid-ocean ridges.

3. Dissolved H_2 Sensor

Dissolved H_2 is a key parameter that can be used to constrain thermodynamic equilibria and kinetic processes during water−rock interactions.[9,49−52] For the mid-ocean ridge vent system, however, dissolved H_2 is virtually the only component that can be directly determined and reliably used to indicate the redox state of the system. Over the years, numerous efforts have been made to measure dissolved H_2 concentrations in hydrothermal fluids utilizing in situ meth-

ods. Chou and Eugster, for example, successfully developed the Ag−AgCl−H_2O H_2 sensor, which is based in part on H_2 permeability through a metallic Pt or Ag−Pd membrane.[53] In their design, H_2 fugacity is indirectly obtained by measuring HCl concentrations of the quench solution in the sensing capsule with a system of Ag−AgCl−HCl. In contrast, a small-volume pressure transducer was coupled to a Ag−Pd membrane permeable to H_2 for measurement of H_2 in hydrothermal experiments.[54−56] A similar approach, but one that makes use of $Au_{50}Pd_{50}$ alloy membrane for chemical stability, also shows great promise in hydrothermal application.[57] Another in situ method for H_2 measurement in high-temperature aqueous systems, however, was developed by Macdonald et al. and makes use of H_2-dependent resistivity of palladium, which serves as the sensor.[58] The response of this sensor to H_2 was demonstrated for dissolved H_2 at concentrations up to 0.72 mmol/kg in 0.1 mol/kg of boric acid and at temperatures as high as 275 °C. The only approach that has been successfully used to measure and monitor dissolved H_2 in high-temperature hydrothermal fluids at mid-ocean ridges is based on the YSZ−pH sensor with a coexisting indicator electrode composed of Pt or Au.[30,59−61]

3.1 Sensor Design and Construction

It is abundantly clear that Pt electrodes are extremely sensitive to changes in dissolved H_2 concentration but respond as well to pH, as indicated in eqs 7 and 8. However, by coupling the H_2 electrode (Pt) with the YSZ−pH electrode, as depicted in cell eq 11, the overall potential of the cell is only a function of dissolved H_2.[30]

$$\mathrm{Pt|H_2, H^+, H_2O|ZrO_2(Y_2O_3)|HgO|Hg} \qquad (11)$$

In the cell illustrated by eq 11, the YSZ−pH electrode actually serves as a reference for H_2 measurement. Therefore, the measured potential is a specific function of the H_2 fugacity (f_{H_2}):

$$\Delta E(V)_{H_2} = \left[E^\circ_{Hg/HgO} + \frac{2.303RT}{2F}\log\left(\frac{f_{H_2}}{a_{H_2O}}\right)\right] \qquad (12)$$

The term f_{H2} can be related to dissolved H_2 by Henry's law, as follows:

$$f_{H_2} = K_H \gamma_{H_2} m H_2 \qquad (13)$$

where K_H, γ_{H_2}, and mH_2 are the Henry's law constant, activity coefficient for H_2, and dissolved H_2 concentration, respectively.[62,63] At a given temperature and pressure condition, the term γ_{H_2} is a function only of ionic strength, which can be determined from experimental and theoretical data.[64,65] Thus, by combining eq 12 and 13, we have a relationship between potential and dissolved H_2 concentration:

$$\Delta E(V)_{H_2} = \left[E^\circ_{Hg/HgO} + \frac{2.303RT}{2F}\log\left(\frac{K_H\gamma_{H_2}}{a_{H_2O}}\right)\right] + \frac{2.303RT}{2F}\log(mH_2) \qquad (14)$$

At a given temperature, pressure, and ionic strength, the term in the squared parentheses of eq 14 is constant and can be calculated from available thermodynamic data.[42,62−68] Thus, the dissolved H_2 concentration can be determined by measuring sensor potential, $\Delta E(V)_{H_2}$. As emphasized throughout, besides being a pH electrode, YSZ also can serve as a reference electrode, which when coupled with a gas sensor (e.g., dissolved H_2), effectively eliminates the pH dependency of the dissolved gas sensor. Indeed, by using this approach, we have had great success with the design and development of a new H_2S sensor, which involves coupling YSZ with an Ag/Ag_2S electrochemical cell.[61]

Platinum is typically the preferred material for the dissolved H_2 sensor owing to the chemical stability of Pt and its effective catalytic capacity facilitating redox reactions involving H_2O. We have found that Pt with even a relatively small surface area (8 × 3 × 0.5 mm) serves well as a hydrogen electrode. In practice, the Pt foil is welded to a Pt wire, which is coated with heat shrinkable polytetrafluoroethylene (PTFE) and in turn placed inside a zirconia tube having 0.8 mm wall thickness. The Pt electrode is then combined with YSZ and secured within the previously described titanium reaction vessel for testing and determination of signal response characteristics.

Experimental studies have also indicated that Pt can be functionally replaced by an electrode made entirely of gold.[59] Gold is especially well suited for studies of the dissolved H_2 in hydrothermal vent fluids because it enjoys unmatched stability in H_2S-bearing fluid and has a much lower H_2 permeability in comparison with Pt.[69−72] A gold electrode, however, has generally been considered unsuitable as an H_2 sensor owing to its electronic structure characterized by an entirely filled d suborbital, which should inhibit the catalytic effectiveness needed for H_2 oxidation.[73−75] Although this may be the case at room temperature and pressures, our research has documented that this is not true at elevated temperatures and pressures where the catalytic effects are enhanced.

3.2 Verification of Sensor Performance

In a manner identical to the previously discussed YSZ pH sensor, the H_2 sensor is also a thermodynamic sensor. Thus, there is no need for calibration. However, its performance can be verified by experimental studies. It is particularly necessary to establish unambiguously that the measured potential is unaffected by fluid pH. In other words, both YSZ and H_2 electrodes respond identically to pH change as imposed by eqs 12 and 14 should be experimentally verified. Apart from procedures designed to test the YSZ−pH sensor, dissolved H_2 concentration in laboratory and field test fluids can be independently determined and well constrained. By sampling the test fluids at elevated temperatures and pressures and then analyzing by GC (gas chromatography), direct verification of the sensor performance can be confirmed.[30,62,76]

Three types of the experiments have been designed for laboratory verification of the H_2 sensor. In each case, we rely on the titanium flow reactor described previously. Since conventional HPLC pumps are not suitable for use with gas-charged fluid, especially H_2, we developed a high pressure and chemically inert separator, which allows us to inject fluid containing different amounts of dissolved H_2 into the reaction vessel at experimental conditions. Thus, the titanium flow reactor in combination with a pressurized and chemically inert gas delivery system provides an ideal means to determine sensor performance characteristics at conditions that simulate the field systems we wish to better understand.

3.2.1. Temperature Constraints on Sensor Response

The experimental fluid with low dissolved H_2 concentration (<0.5 mmol/kg) is first heated from room temperature

to 350 °C to examine the effect of temperature on electrode response. During heating, pressure can be maintained constant at 400 bar by proportionally releasing fluid from the reactor through a computer-actuated metering valve. Our results indicate that temperatures greater than approximately 150 °C are required before the sensor begins responding to dissolved H_2 (Figure 8).[59] It is quite possible that this

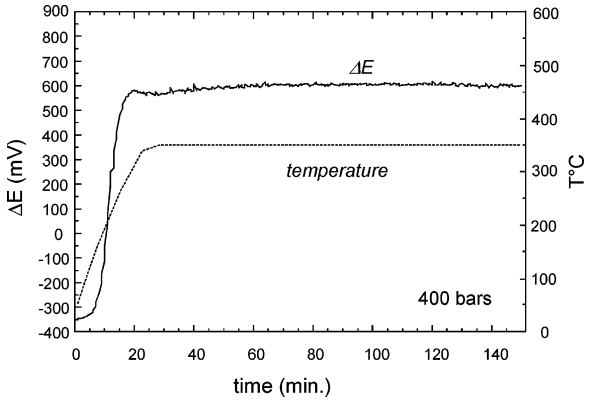

Figure 8. Measured potential ($\Delta E(V)$) of the Au-YSZ(Hg/HgO) electrochemical cell from heating experiments at temperatures up to 350 °C (modified after ref 59). The dashed line indicates changes in temperature during the experiment. Results show that temperatures >150 °C are needed to overcome temperature-dependent conductivity constraints imposed by the YSZ ceramic (see text).

"temperature barrier" is caused chiefly by the well-known ion conductivity constraints imposed by the YSZ ceramic membrane,[27,29] although inherent limitations of the gold indicator electrode also cannot be ruled out.

3.2.2. Reversibility

The reversibility of the H_2 sensor is best determined by conducting experiments in which the concentration of dissolved H_2 in fluid coexisting with the YSZ−Au electrodes is changed or regulated, while fluid samples are periodically removed and analyzed for dissolved H_2 by GC techniques. For this experimental test, deionized water (H_2-free DIW) or H_2-bearing solution is introduced into the titanium flow-reactor to decrease or increase, respectively, the dissolved H_2 concentration. These procedures are performed at constant temperature, pressure, and fluid flow rate (0.5 mL/min.). Thus, using this approach, data on the rate of response of the sensor to dissolved H_2 have been obtained. For example, flow-through experiments at 350, 375, and 400 °C, for both Pt- and Au-based sensors, reveal rapid and reversible response to changes in dissolved H_2 (Figures 9 and 10).[30,59] Indeed, at 400 °C, changes in dissolved H_2 ranging from 0.02 to 0.6 mmol/kg, are virtually instantaneous and matched by corresponding changes in the measured in situ cell potential. These tests show that the H_2 sensor responds effectively to H_2 concentrations in fluids at elevated temperatures and pressures, which underscores the potential of the sensor for further development and eventual deployment at seafloor hydrothermal vents.

3.2.3. Nernstian Response

Consistent with constraints imposed by eq 12, sensor response to dissolved H_2 needs to be more than rapid and reversible; it also needs to follow Nernst law predictions. Thus, experiments were performed as before, but additional efforts were made to ensure that equilibrium was achieved.

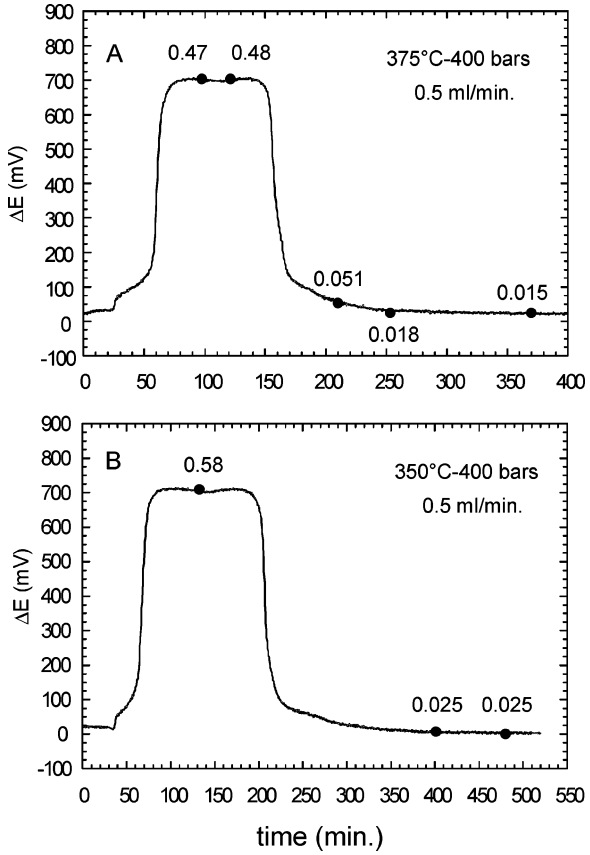

Figure 9. Measured potential ($\Delta E(mV)$) of H_2 sensor recorded during flow-through experiments at 375 °C (in A) and 350 °C (in B) (modified after ref 30). The pressure and flow rates are 400 bar and 0.5 mL/min, respectively. The dissolved H_2 concentrations obtained from GC analyses are also indicated, which demonstrate an excellent consistency with in situ measurements (potential). The numbers above the solid dots are corresponding dissolved H_2 concentration measured by GC.

This was accomplished by systematically changing dissolved H_2 while simultaneously monitoring the in situ signal response of the H_2 sensor. In particular, sensor readings for the same dissolved H_2 concentrations were repeatedly achieved and reversed in compositional space throughout the experiment, while temperature and pressure conditions were maintained at constant.

Tests have now been performed with dissolved H_2 concentrations ranging from 0.18 to 4.05 mmol/kg at supercritical conditions (400 °C−400 bar).[30,59] This range of dissolved H_2 concentrations is analogous to values expected for natural systems and includes relatively oxidizing conditions, buffered by hematite−magnetite−fluid equilibria, as well as more reducing conditions, buffered by pyrrhotite−pyrite−magnetite−fluid equilibria.[52,62,63,77] The anticipated linear relationship between in situ measured sensor potential and the logarithm of the dissolved H_2 concentration was obtained for both Pt- and Au-based sensors. For example, at 400 °C, experimental data for the Au sensor reveals a slope of 0.0670 ± 0.0027 (Figure 11), as follows:

$$\Delta E_{\mathrm{YSZ,Au}}(V) = 0.9822(\pm 0.0080) + 0.0670(\pm 0.0027) \log m\mathrm{H_2(mol/kg)} \quad (15)$$

The agreement with the predicted Nernstian slope of 0.0668 is excellent.[59] A similar response has been determined for the Pt−H_2 sensor.[30] The agreement between experimental

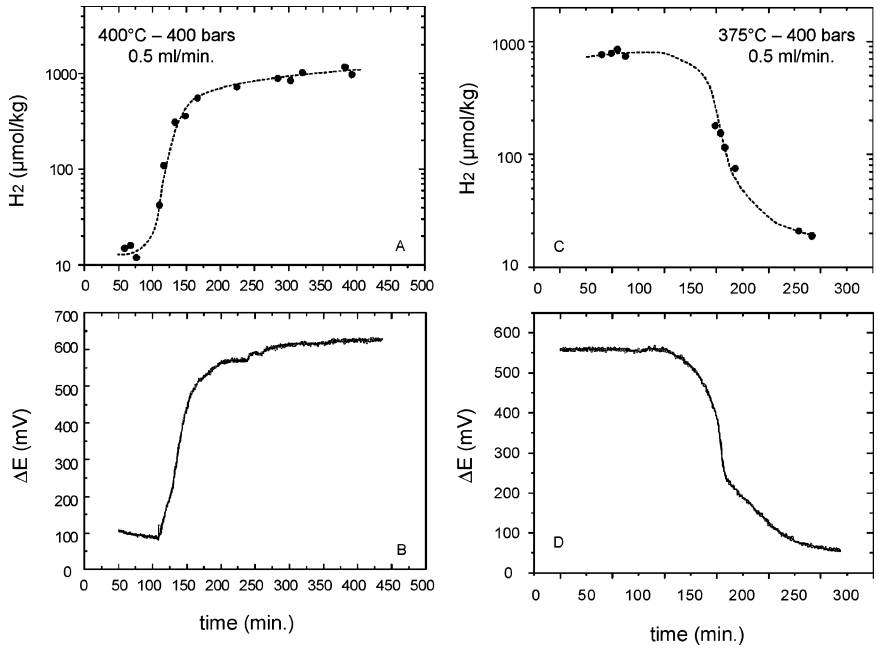

Figure 10. Measured potential ($\Delta E(mV)$) of the Au-YSZ(Hg/HgO) electrochemical cell to dissolved H_2 concentrations as demonstrated by flow-through experiment (flow rate of 0.5 mL/min) at 400 bar (modified after ref 59). The results obtained from 375 °C are plotted in C and D, while those from 400 °C are shown in A and B. Changes in dissolved H_2 were initiated by constantly decreasing or increasing H_2 concentration in the fluid (see text). The dissolved H_2 concentrations were measured by GC.

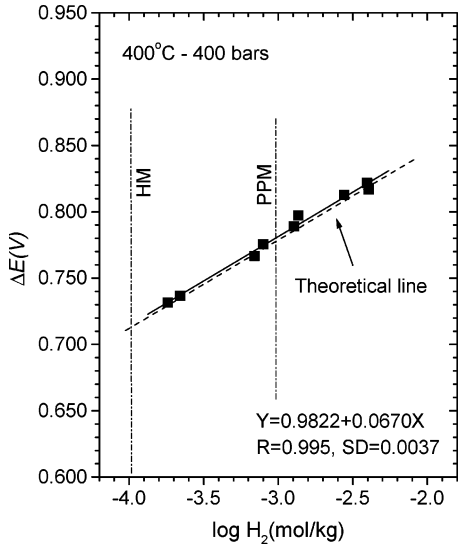

Figure 11. Measured potential ($\Delta E(V)$) as a function of dissolved H_2 concentrations in aqueous fluid at 400 °C and 400 bar (modified after ref 59). Solid symbols represent measured data from the sensor based on Au-YSZ(Hg/HgO) electrochemical cell. Dashed lines indicate dissolved H_2 concentrations from hematite-magnetite (HM), and pyrrhotite−pyrite−magnetite (PPM) assemblages, which represent the most common dissolved H_2 range in hydrothermal systems, especially in mid-ocean ridge. Results reveal excellent Nernstian response defined by the in situ potential and coexisting dissolved H_2 concentrations.

and theoretical data clearly indicates that overall equilibrium was achieved, in a manner consistent with eqs 12 and 14, while once again providing additional evidence that the H_2 electrodes (Au, Pt) and the YSZ electrode respond identically to fluid pH, a point that cannot be overemphasized, since it confirms an underlying assumption intrinsic to the fundamental or primary nature of the YSZ−pH sensor.

To constrain better the overall performance of the H_2 sensor, the Y-intercept defined by eq 15 can be evaluated in comparison with theoretical data for the standard potential ($E^\circ_{Hg/HgO,T}$) and the Henry's law constant for H_2 (K_H), as described by eq 13. On the SHE scale, $E^\circ_{Hg/HgO,T}$ is 0.8522 V at 400 °C based on thermodynamic data for Hg, H_2O, and $H_{2(g)}$ from Naumov et al.,[66] Haar et al.,[67] and Johnson et al.,[42] respectively. In comparison, $E^\circ_{Hg/HgO,T}$ calculated from data in Robie et al.[68] is 0.8505 V. Similar values can be regressed for the entire range of experimental conditions studied, which lends confidence to the thermodynamic underpinnings essential for applications based on eqs 12 and 14. As for the Henry's law constant for H_2 (K_H), we used data from Kishima and Sakai,[62] which at 400 °C and 400 bar yields a log value of 1.90. This is also in very good agreement with the analogous data from Shock et al.[65] at the same conditions. Finally, considering the relatively low dissolved concentrations of ionic aqueous species in the experimental fluids, a_{H_2O} and γ_{H_2} can be taken to be unity. Thus, at 400 °C and 400 bar eq 14 can be rewritten as follows:

$$\Delta E(V) = 0.9788 + 0.0668 \log m\mathrm{H_2}(\mathrm{mol/kg}) \quad (16)$$

This numerical relationship (slope and intercept) agrees well with the experimentally derived data depicted by eq 15. Thus, the dissolved H_2 sensor, especially constructed with an Au-based sensing element, is well suited for determining dissolved H_2 concentrations of aqueous fluids at elevated temperatures and pressures.

4. In Situ Measurements at Seafloor Hydrothermal Vents

The laboratory demonstration of the effectiveness of YSZ-based solid-state chemical sensors for the in situ determination of pH and dissolved H_2 in high-temperature chloride-bearing hydrothermal fluids provides the requisite justification for the development of a unit that can be deployed at seafloor vents. However, at seafloor hydrothermal vent sites, conditions confronted are difficult or impossible to simulate in the laboratory. The most obvious difference is related to the

need for deployment in very restricted spatial geometries in an environment characterized by unusually large thermal gradients (>100 °C/cm). Accordingly, new strategies are needed to permit sensor related studies of subseafloor hydrothermal fluids using manned-submersible (HOV) and/or remotely operated vehicle (ROV) assets. Thus, in recent years, extraordinary efforts have been dedicated to transforming the laboratory-based chemical sensor technology into an instrument package capable of seafloor deployments. These developments have been enhanced by the construction and testing of an array of chemical sensors, which can be deployed autonomously to conduct in situ measurements of pH, H_2, and H_2S concentrations in hydrothermal vents on the seafloor.

Following preliminary field tests in 1998,[78] the first successful measurements of in situ pH and dissolved H_2 in the hydrothermal fluids were made with newly developed sensor units at a number of vent sites on mid-ocean ridges. The deployments now cover more than 10 high-temperature vent sites on three different ridge segments, including the Main Endeavour Field of Juan de Fuca Ridge (47° 57′ N, 129° 06′ W), EPR 21°N and 9−10°N through four cruises over a range of 6 years. The hydrothermal vents investigated are at the depth of approximately 2200 and 2500 m, respectively, and issue fluids at the temperature up to 380 °C.[34,61] The results obtained from these studies are consistent with those predicted or determined from alternative approaches, as reviewed below.

4.1. Sensor Unit Design for the Seafloor Deployment

A seafloor deployable sensor system must be a self-contained unit, which includes the capacity for simultaneous measurement with multiple chemical and temperature sensors, configured in such a way so as to enhance chemical sensitivity and specificity. In addition, the sensor unit must contain a reliable power supply and an electronics system for signal processing and real time data communication. In the case of autonomous deployment, the unit must also be designed to operate with low power consumption characteristics and permit sufficient data storage to support unattended long-term monitoring applications. Important advances in the integration of thermal and electrochemical sensors in a small, chemically resistant, and well-protected unit some distance from the pressure sealed electronics and system control components have greatly enhanced the utility and performance of the sensor system for challenging seafloor applications.

4.1.1. Mechanical Considerations

In general, the sensor unit consists of three subsections or components: (1) the electrode assembly unit; (2) the transition assembly; and (3) electronics package (Figure 12). Titanium alloy (6Al4V) is used in the construction of virtually all system components owing to the well-known physical and chemical characteristics of this material.

The electrode assembly unit is located at the most forward region (tip) of the sensor and housed in a titanium casing, which was designed to enhance the flow of fluid past the electrodes, while at the same time protecting the electrodes from potential impact with rock or chimney structures. The outer diameter of the electrode assembly unit is 2.5 cm. A distance of less than 0.5 cm separates all electrodes, including a titanium-sheathed J- or E-type thermocouples constructed

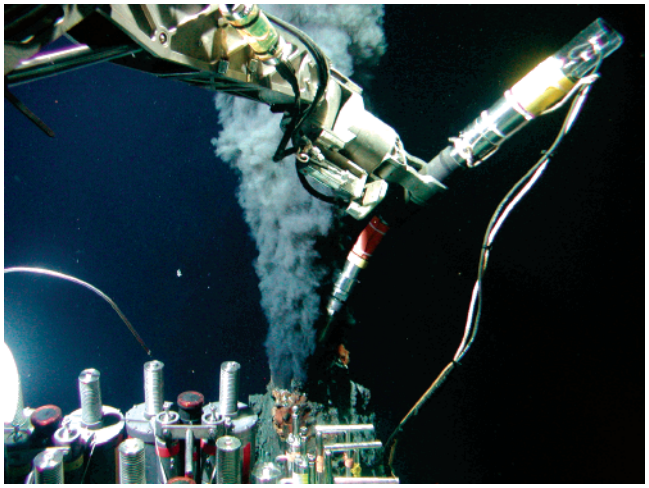

Figure 12. Integrated array of chemical sensors designed and developed for subseafloor studies of the chemistry in hydrothermal fluids using manned submersible assets (*DSRV ALVIN*). The picture shows deployment of the sensor unit at SW vent of 21°N EPR during Alvin dive 3749. Reprinted with permission from ref 34. Copyright 2005 Elsevier.

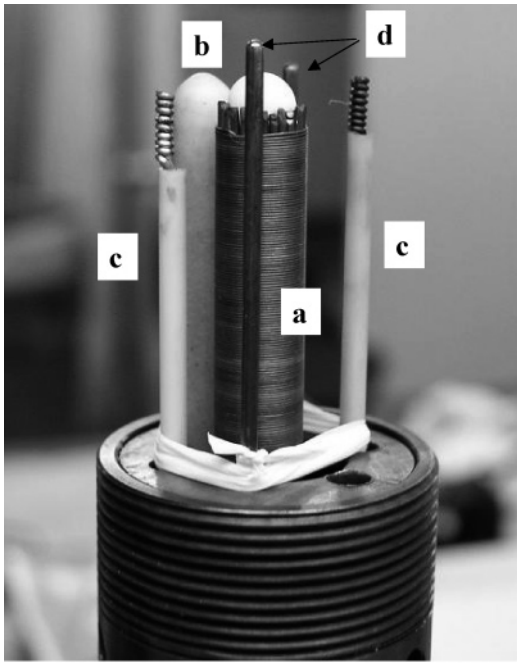

Figure 13. A close-up illustration of sensor configuration, which includes the YSZ−pH sensor (a), reference electrode (b), dissolved gas sensors (c), and as well as thermocouples (d) (see text).

by Entherm (Bloomington, MN). These thermocouples are characterized by low uncertainties (±1.7 °C for type-E, ±2.2 °C for type-J) over the range of temperatures encountered at hydrothermal vents (Figure 13). Importantly, the response region of the electrodes is limited to <0.6 cm from the tip of the assembly unit, which allows precise control of chemical measurements in specific thermal regimes in vent fluid systems. The electrode assembly is pressure sealed using a modified Conax fitting and associated viton sealant (Conax Buffalo, NY), effectively precluding penetration of seawater or vent fluid into the other subunits of the sensor system (Figure 14).[79]

The transitional section functions as a conduit for protecting electrical connections between the temperature, electrochemical sensors, and the electronic compartment from

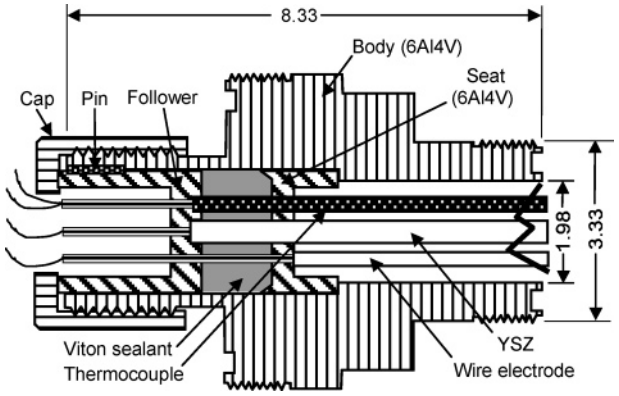

Figure 14. Schematic diagram depicting the seal mechanism used for electrodes and thermocouples in the sensor system. Units are in cm. Reprinted with permission from ref 79. Copyright 2006 IEEE.

seawater penetration. The unit is constructed in such a way so as to provide an effective shield for the high impedance and low voltage signals generated from the chemical sensors against possible signal interference from other electrical operations involved with seafloor deployment. Viton O-rings are used as pressure sealants as with the other two subsections. The reinforced metal casing of the transition unit, however, also serves as a convenient means for gripping the sensor unit by hydraulically activated manipulators inherent to submersible operations by which seafloor deployments are made possible. In terms of seafloor deployment strategies, we have recently integrated the sensor unit with a hydraulic ram that can remotely control the movement and positioning of the sensor on the seafloor (Figure 15). For more effective

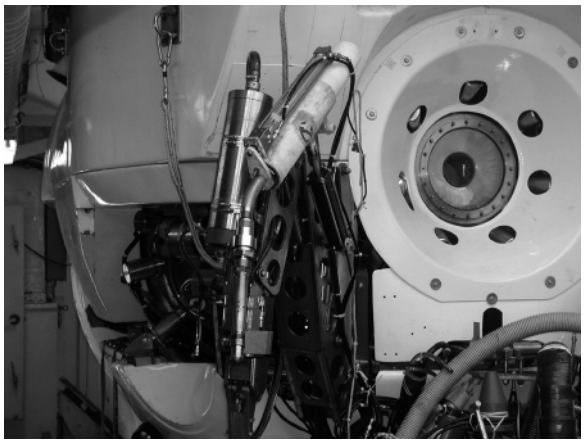

Figure 15. Chemical sensor system installed directly onto the manipulator of *DSRV ALVIN* prior to use for real time measurements of pH and selected dissolved gases in subseafloor hydrothermal fluids.

access to hydrothermal vent fluids issuing from chimney structures or accumulating beneath overhanging seafloor sulfide structures (flanges), the transition assembly is bent to allow tilting the front end of the sensor unit at a 30° angle (Figure 12).

The electronics package subunit is contained in a cylindrical casing (20.32 cm (l), 7.30 cm (o.d.), and 2.70 cm (wall thickness)), which is also constructed of Ti-alloy. This subunit contains all requisite electronics components and batteries for signal processing, data storage, and data transmission. The total length of the fully assembled sensor unit is approximately 1 m and weighs less than 5 kg (in water).

4.1.2. Electronics and Data Communication

The electronics package involves three internal subsystems: an electrometer for processing high impedance (up to 10^{14} Ω) DC voltage from the chemical sensor, an analogue to digital converter, and a microcomputer to scan chemical sensor and temperature input (channels) and to permit communication with the deployment vehicle (Figure 16).

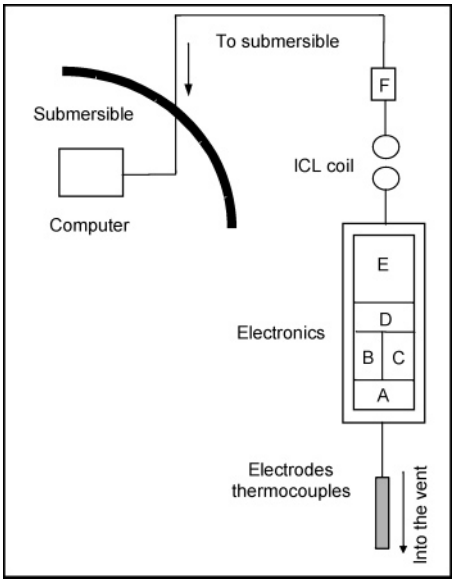

Figure 16. Schematic diagram showing electronics package of the sensor system and the connection between the sensor and the submersible. The letters indicate the following components. (A) the electrometer for processing high impedance DC voltage from the sensor; (B) the analogue to digital converter; (C) the microcomputer; (D) the internal ICL modem to transfer out the signal via a pulsed magnetic field; (E) battery pack (7 AA cells) for powering the system; (F) the external ICL modem for facilitating true RS-232 communication with the computer inside of the submersible.

Data transfer is accomplished by inductively coupled link (ICL),[80] while seven AA cells power the system. The power consumption is only 23 mA, and the unit shuts down if not called upon within 1 min. In "sleep" mode the unit requires as little as one microwatt of power. In general, the ICL interface allows noncontact communication between the submersible and the sensors (thermal, chemical) via a pulsed magnetic field from a simple coil of wire at any baud rate up to 9600. The ICL system uses two or more magnetic coils (links) with associated electrical interface, which serve as modems. Two types of modems exist, one that interfaces to a computer inside the deployment vehicle via true RS-232 communication, and another built into the electronics package of the sensor unit. The modem internal to the sensor contains a 5v CMOS interface to minimize power consumption. The modems operate using an unregulated power supply providing between 8 and 15 V. Separation between the magnetic loops can be as great as 10 cm at 12 V, although actual operations are conducted at distances always considerably less than this. Use of inductive loops provides total electrical isolation between the sensor and the deployment vehicle. Since it is possible to deploy more than one inductive link, simultaneous data transmission from multiple chemical sensors is possible simply by uniquely addressing each unit. The computer software for sensor operations was developed with LabView code, allowing real time data acquisition and processing at a sampling rate of 3∼5 s per reading.

4.2. In Situ pH Measurement

Sensor measurements at seafloor hydrothermal vents have been made using two distinct deployment strategies. The first involves pH measurement of the highest temperature fluids at each of the vent sites in an effort to obtain the hydrothermal end-member (source fluid) pH values. This objective was greatly aided by the presence of two Ti-sheathed thermocouples immediately adjacent to the pH sensor. These thermocouples provide real-time temperature data, while the sensor is positioned in the vent fluid. Temperature maxima are typically achieved when the tip of the sensor is placed on top of the orifice or in contact with the inside wall of the chimney, approximately 2−3 cm beneath the orifice. In the case of flange pools (accumulations of hydrothermal fluid trapped beneath overhanging chimney structures, especially at the Main Endeavour Field (MEF)), the highest temperatures are encountered when the sensor is inserted as deeply as possible into the pooled fluid with the tip held against the underside of the flange.[61] The second deployment strategy is designed to trace changes in pH during cooling, mixing, and mineralization of the end member hydrothermal fluid with seawater. This is accomplished by gradually moving the sensor tip from the interior to exterior of the fluid issuing from the vent orifice.

4.2.1. Sensor Response

Real-time temperature and in situ pH sensor data (mV) obtained for endmember hydrothermal vent fluids issuing from high-temperature vents demonstrate rapid response and also outstanding stability (Figures 17 and 18). In general, the sensor Emf signal stabilizes in less than 5 min but always after stabilized temperature readings are obtained. To avoid thermal shock during the placement of the sensor head in hot hydrothermal fluid, a gradual and incremental movement of the sensor along the thermal gradient is often necessary, as shown by the temperature trace recorded by the sensor (Figure 17). The reversibility of sensor data can usually be verified by re-establishing steady-state temperature and sensor data during deployment. For instance, at Dante vent site (MEF), sensor and temperature data reveal repeated stability at similar values subsequent to overcoming the effects of intermittent episodes of seawater incursion into the venting hydrothermal fluid (Figure 18).

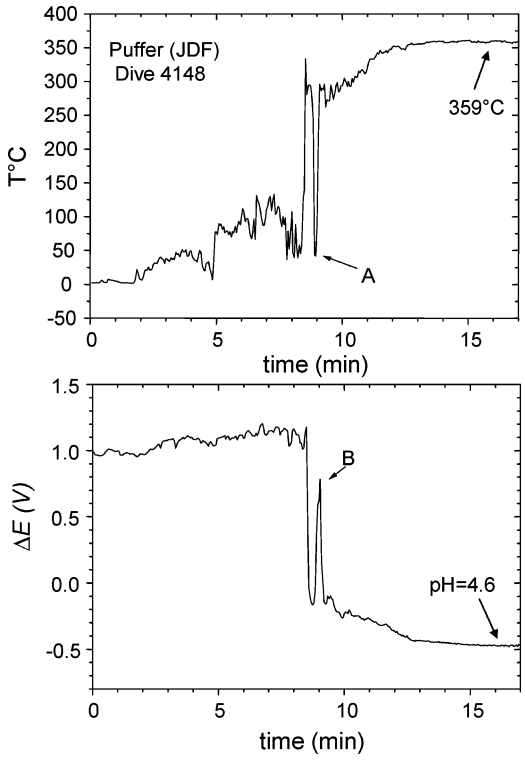

Figure 17. In situ sensor potential ($\Delta E(V)$) recorded in real time during pH measurement of hydrothermal fluid at Puffer vent site (MEF, Juan de Fuca Ridge) in 2005 during dive 4148. Data clearly demonstrate the rapid rate of response of sensor potential ($\Delta E(V)$) to the fluid pH. Changes in temperature caused by the mixing with seawater (A) were also reflected almost instantaneously by the recorded sensor signal (V) (A and B).

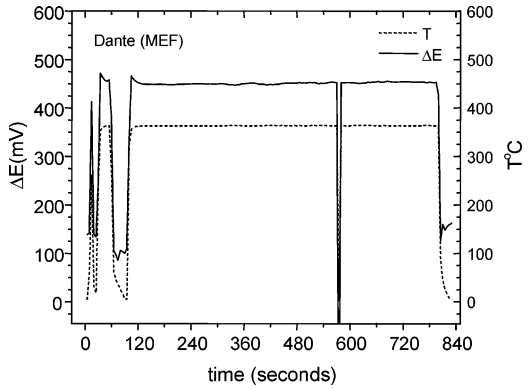

Figure 18. Temperature of fluid issuing from the flange pool at Dante vent site (MEF) (dotted line) in comparison electrochemical data ($\Delta E(mV)$) determined by YSZ−pH sensor (solid line). The solid line indicates $pH_{(in-situ)}$ at the corresponding temperature. By systematically positioning the sensor in the flange pool, stable chemical (pH) and thermal response is achieved, although a sudden infusion of cold seawater (∼2 °C) at the 560 s interval resulted in a sharp drop in both temperature and mV output. Immediately following this, however, the signals returned to the previously established steady-state condition, which provides additional insight of the response time and reproducibility of the YSZ−pH sensor. Reprinted with permission from ref 34. Copyright 2005 Elsevier.

4.2.2 Uncertainties with the In Situ pH Value

pH values are determined from sensor and temperature data after readings achieve steady-state values, which are indicated by variability of ∼ ±0.004 V and ± 3 °C for $\Delta E(V)^{\circ}_{T,P}$ and T, respectively. Thus, for pH data obtained at 400 °C, the inherent uncertainties associated with Emf variation are less than ± 0.03 pH units. As indicated earlier, however, dissolved Cl concentration is also a necessary consideration owing to constraints on $a(Cl^-)$ imposed by the reference electrode (eq 6). Uncertainties involving this parameter will contribute to errors in the pH data, although the form of the Nernst equation mitigates the magnitude of this. For instance, even with an uncertainty of ±50 mmol/kg in total dissolved Cl concentration, the corresponding variation in the $pH_{(in-situ)}$ value is only ±0.02 pH units. However, it is unlikely that this extreme case could apply on the time scale of vent fluid measurements. The other factor that may affect $a(Cl^-)$ is the uncertainty associated with the association constant of $NaCl_{(aq)}$, the dominant Cl-bearing aqueous species in hydrothermal vent fluids. For instance, at 400 °C and 400 bar, available thermodynamic data[8,42,45] for $NaCl_{(aq)}$ reveals variation of 0.224 log units, which corresponds to a difference of ∼0.04 units in the determined $pH_{(in-situ)}$ values (Table 2). Although these uncertainties are not particularly serious, all reasonable efforts need to be made to minimize errors when recognized. At present time, no other direct method is available for determining in situ pH

Table 2. Comparison between the in Situ pH Values Obtained from the Sensor Measurement and Theoretical Calculation for 0.57 mol/kg NaCl−HCl System at 400 °C and 400 bar

experiment	YSZ-1	YSZ-2	YSZ-3
$pH_{(25^\circ C)}$	2.96	3.55	3.63
$\Delta E(V)$	-0.478 ± 0.001	-0.406 ± 0.004	-0.399 ± 0.003
$pH_{(in-situ)s}$ [a]	4.66 ± 0.01	5.20 ± 0.03	5.25 ± 0.02
$pH_{(in-situ)calc}$ [b]	4.66	5.25	5.33
$\Delta pH_{(in-situ)}$ [c]	0	0.05	0.08
$pH_{(in-situ)h}$ [d]	4.62 ± 0.01	5.18 ± 0.03	5.21 ± 0.02
$\Delta pH_{(in-situ)h}$ [e]	0.04	0.04	0.04

[a] The pH data determined based on the sensor measurement ($\Delta E(V)$) and the thermodynamic data for NaCl from SUPCRT92.[42] [b] Predicted data using the revised HKF equation and associated database.[13,41,42,44] [c] The difference between $pH_{(in-situ)s}$ and corresponding $pH_{(in-situ)calc}$. [d] The pH data determined based on the sensor measurement ($\Delta E(V)$) and the thermodynamic data for $NaCl_{(aq)}$ from Ho et al.[45] [e] The difference between $pH_{(in-situ)s}$ and corresponding $pH_{(in-situ)h}$.

at elevated temperature and pressure condition in the NaCl−H_2O system relevant to mid-ocean hydrothermal fluids. This situation is distinct from that of dissolved H_2, where in situ data can be directly verified by simultaneous acquisition of gas-tight fluid samples followed by GC analysis. To assess the accuracy of $pH_{(in-situ)}$ measurements, however, comparison with theoretically predicted data is most useful. In Table 2, we made such a comparison at the chemical and physical conditions applicable to the seafloor vent system. As indicated, the precision of the measured potential is $\sim \pm 0.004$ V (1σ), which results in a corresponding uncertainty of approximately 0.03 pH units. The difference between in situ pH values and equivalent data predicted from distribution of aqueous species calculations is ≤ 0.08 pH units. Therefore, if we choose the theoretically predicted value as the standard means of comparison, the overall uncertainty in the pH value obtained from the in situ measurement is in a range of 0.01−0.10. It is necessary to emphasize, however, that error analysis of this sort is necessarily model dependent, and as the thermodynamic data for dissolved aqueous species are refined so too will be the magnitude of offset between field and/or experimental data and constraints imposed by results of theoretical models. In general, the assessment of uncertainties from our pH measurements in chloride-bearing fluid at elevated temperatures and pressures is similar to estimates made by Lvov et al.,[15,27] in which a YSZ pH-sensing electrode was used with a flow-through external pressure-balanced reference electrode (EPBRE) to measure the pH of moderately dilute fluid at high temperature and pressures. This uncertainty level certainly represents an important improvement over that of the theoretical prediction for in situ pH of seafloor vent fluids. It is difficult to account for the full chemistry of the vent fluid in the speciation accurately, as a large number of the available dissociation constants are with an error of 0.3−0.7 log units,[44] and not all of the necessary constants are available. Although the lowest possible uncertainty is required for pH measurement of seafloor hydrothermal vent fluids at elevated temperatures and pressures, since small changes in fluid pH can induce large changes in coexisting geochemical systems, further improvements will likely need to wait advances in theoretical models depicting the distribution aqueous species at unusually challenging chemical and physical conditions, supplemented by results of laboratory investigations where these models can by unambiguously tested.

4.2.3. Verification of the Vent Fluid $pH_{(in-situ)}$

In general, vent fluids with high measured temperatures have high $pH_{(in-situ)}$ values. For example, P-vent fluid (9°50′N EPR) and Dante and Hulk vent fluids (MEF, JDF) have temperatures and $pH_{(in-situ)}$ of 384°, 362°, and 337 °C, and 5.4, 5.3, and 4.4, respectively (Figure 19).[34] These data are

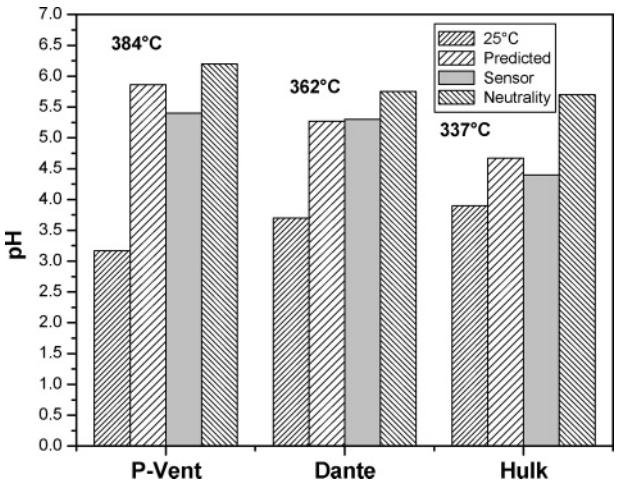

Figure 19. Measured $pH_{(in-situ)}$ in comparison with calculated $pH_{(in-situ)}$ for selected vent fluids from the MEF (Hulk, Dante) and EPR 9°50′N (P-vent). In the legend, 25 °C, predicted, sensor, and neutrality represent the values of measured $pH_{(25^\circ)}$, calculated $pH_{(in-situ)}$, measured $pH_{(in-situ)}$, and pH neutrality at the corresponding condition, respectively. As shown, $pH_{(in-situ)}$ values increase with increasing temperature, but remain considerably more acid than neutrality at all conditions investigated. Dissociation of H^+-bearing aqueous species and mineralization effects combine to render $pH_{25^\circ C}$ acidic. When these effects are accounted for using available thermodynamic data at appropriate P−T conditions, however, agreement between pH predicted at elevated temperatures and pressures and measured in situ is generally within $\pm 0.1-0.4$ units. Reprinted with permission from ref 34. Copyright 2005 from Elsevier.

generally consistent with results predicted from experimental and theoretical studies, as marked with a shaded area in Figure 7. The in situ measurements, especially those conducted at vents issuing fluid at temperatures higher than 350 °C, confirmed the theoretical prediction that pH values in the vicinity of 5 are most consistent with phase equilibria constraints at conditions likely for subseafloor reaction zones from which the vent fluids are ultimately derived.[7−9,81,82]

To illustrate this further, $pH_{(P,T)}$ values were calculated and compared with those obtained from sensor measurements. As shown in Figure 19, the difference between $pH_{(in-situ)}$ calculated and that actually measured in situ tends to be in the range of 0.1−0.4 units. Although the agreement is especially good for vent fluids at Dante and Hulk (MEF), the offset is greater for hydrothermal fluids issuing from P-vent (EPR 9°N). This may be due to a combination of factors including uncertainties in available thermodynamic data, together with the lack of thermodynamic data for aqueous species in P-vent fluids at the requisite temperature and pressure conditions where the omission of such species may be particularly critical to pH calculation. In sharp contrast with the relatively high $pH_{(in-situ)}$ values, $pH_{(25^\circ C)}$ for the quenched fluid sample is less than 4.0 in all cases (Figure 19). This is obviously a result of the previously described dissociation of H^+-bearing aqueous complexes with cooling during sample processing,[8,9,52,83] which further

demonstrates the advantage of in situ pH measurements determined directly on high-temperature vent fluids.

In addition to constraining the pH of end-member vent fluids, in situ pH data permit assessment of seawater-hydrothermal fluid mixing—a process that is of fundamental importance to mineralization, heat and mass transfer[84,85] as well as the existence of pH-sensitive microbial communities inhabiting seafloor chimney structures and underlying mounds.[86−90] Thus, by incrementally moving the pH sensor from the vent orifice through the interface between hydrothermal and seawater dominated environments, insight into pH-controlling reactions associated with the compositional and thermal evolution of the vent fluid is obtained. Comparing the pH−temperature trend to neutrality at corresponding temperatures shows that mixing and cooling increase fluid acidity, especially at intermediate temperatures (250−300 °C). Theoretical modeling predicts a "U-shaped" pattern, while plotting $pH_{(in-situ)}$ measurements against the corresponding temperature (solid line in Figure 20).[2,37,91,92] This

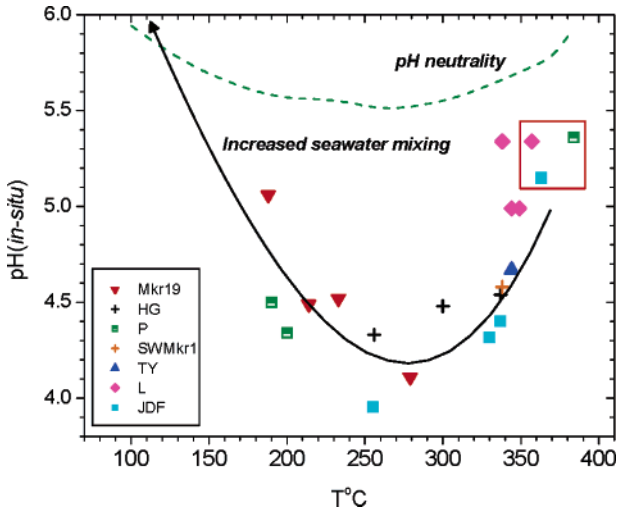

Figure 20. $pH_{(in-situ)}$ plotted against temperature for vent fluids from a wide range of axial locations. All cross symbols represent measurements from the vents at 21°N EPR; data from the Main Endeavour Field (JDF) are shown as solid squares, while all the other symbols indicate data from the vents at 9−10°N EPR. The JDF data, however, specifically refer to vent fluids at Bastille, Hulk, and Dante sites. Other individual vent sites are as indicated in the figure legend: Mkr19 is for Mark 19; HG for Hanging Garden; P and L for P and L vents; SWMkr1 for Marker 1 at SW vent; TY for TY vent. If more than one data points are plotted for a given site, the one with the higher temperature is more closely associated with the center of the vent orifice. The dash line enclosed box at relatively high-temperatures shows previously predicted pH values for end member fluids. The "U-shaped" pattern exhibited when $pH_{(in-situ)}$ is plotted against temperature results from seawater mixing as suggested by theoretical modeling studies.[2,37] Limited mixing effects cause dissociation of H^+-bearing complexes and metal sulfide precipitation, increasing fluid acidity. Greater degrees of mixing, result in seawater-dominated conditions with attendant pH increase (arrow trajectory) and temperature decrease. Reprinted with permission from ref 34. Copyright 2005 from Elsevier.

prediction is consistent with results actually measured (Figure 20). The pH minimum demonstrated here is likely the result of dissociation of H^+-bearing aqueous species and precipitation of pyrite and pyrrhotite from vent fluid derived dissolved Fe and H_2S, as can be simulated from theoretical considerations.[9,83,85,92] Although modest amounts of seawater mixing with vent fluid encourages precipitation of these phases, dilution and oxidation effects associated with greater seawater mixing ultimately limit mineral precipitation, resulting in seawater dominated conditions and relatively high pH, as observed.

4.3. In Situ Dissolved H_2 Measurements

Application and testing of the dissolved H_2 sensor have been carried out simultaneously with in situ pH sensor deployment at hydrothermal vent sites. The successes with pH sensor measurements in the high-temperature vent fluid also set the groundwork for dissolved H_2 sensor measurements. As discussed previously, the operational characteristics of the H_2 sensor are predicated on pH response, since one depends on the other by the design of the electrochemical cell that we use. Where in situ pH data require explicit knowledge of dissolved chloride, however, the same is not necessarily the case for the dissolved H_2 sensor, since $\Delta E(V)_{H_2}$ is independent of the knowledge of other chemical species dissolved in the fluid (eq 12). Hence, the errors that contribute to sensor data from field measurements are reduced. Another advantage unique to the dissolved H_2 sensor is that the measurement can be independently and unambiguously corroborated by analytically processing fluid samples taken at the same time that the sensor data are obtained.[10,12,93,94] With these benefits, however, it is still necessary to bear in mind that the slope of the line depicting Nernstian response (eq 12) is half that of pH, which tends to cause doubling uncertainties in reported H_2 concentrations from in situ Emf measurements. For example, an uncertainty of ±0.003 V, which is generally associated with sensor measurements in aqueous fluids at 400 °C, results in a corresponding precision in dissolved H_2 of approximately 0.05 log units. By comparing the measurement with GC analysis (see eqs 15 and 16), an accuracy value of ∼0.04 log units can also be given to measured data at 400 °C for a concentration range of 4.0−0.1 mmol/kg, which corresponds to an error of approximately 10%.

4.3.1. Field Verification

At present, the dissolved H_2 sensor has been used in hydrothermal vent fluids at temperature and pressure conditions up to 380 °C and 250 bar, respectively.[61] The performance of the sensor is similar to what we have experienced with the pH sensor, allowing for sensitivity variations. Accordingly, the sensor responds rapidly and reversibly to vent fluid chemical and physical data. For example, measurements conducted in a flange pool at Cantilever vent in 1999 over a period of 20 min reveal systematic co-variability of H_2 and fluid temperature, entirely in keeping with experimental and theoretical constraints. Indeed, as demonstrated by traces "B" and "E" in Figure 21, in situ measurements of H_2 reveal steady-state values that correspond well with steady-state temperatures. This is confirmed further by trace "C" (Figure 21), which records a rapid reversal in temperature (370°−210°−370 °C) and corresponding change in Emf response for the H_2 sensor changes that were triggered by a slight repositioning of the sensor tip at the vent/seawater interface, where thermal and chemical gradients are unusually large. Figure 21 also shows that at temperatures less than 125 °C, chemical and temperature measurements are not in phase, indicating the lower temperature limit for sensor response, which likely results from the increasingly higher input impedance of YSZ ceramic and surface reaction barrier of Au with decreasing temperature, in keeping with previous experimental results.[27,29,74]

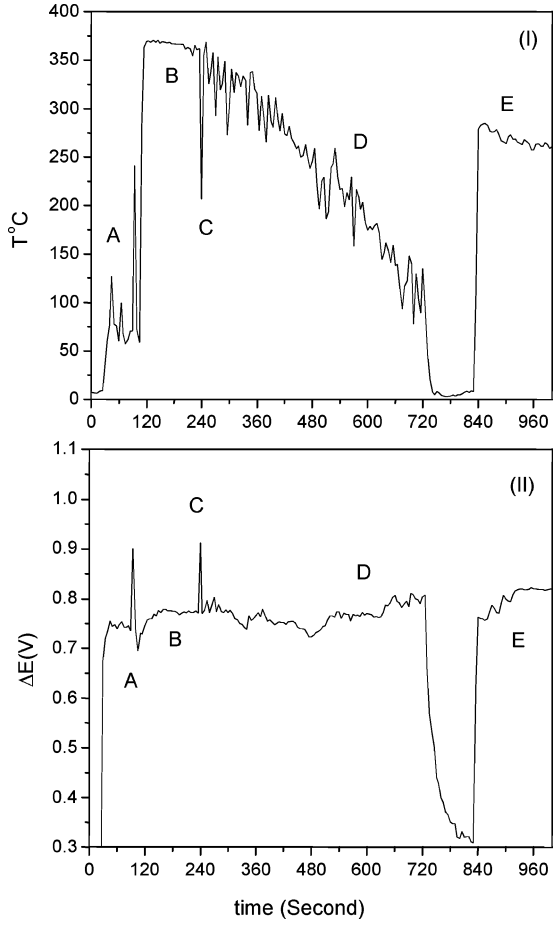

Figure 21. Examples of temperature and dissolved H_2 sensor signals $\Delta E(V)$ obtained in a real time mode during Alvin dive 3474 in 1999 at flange pool at Cantilever (modified after ref 61). Temperature data are plotted in the time sequence shown (I), while data for dissolved H_2 are simultaneously shown in (II) with the same time sequence. Data are labeled with letters from (A) to (E) for easy comparison and discussion.

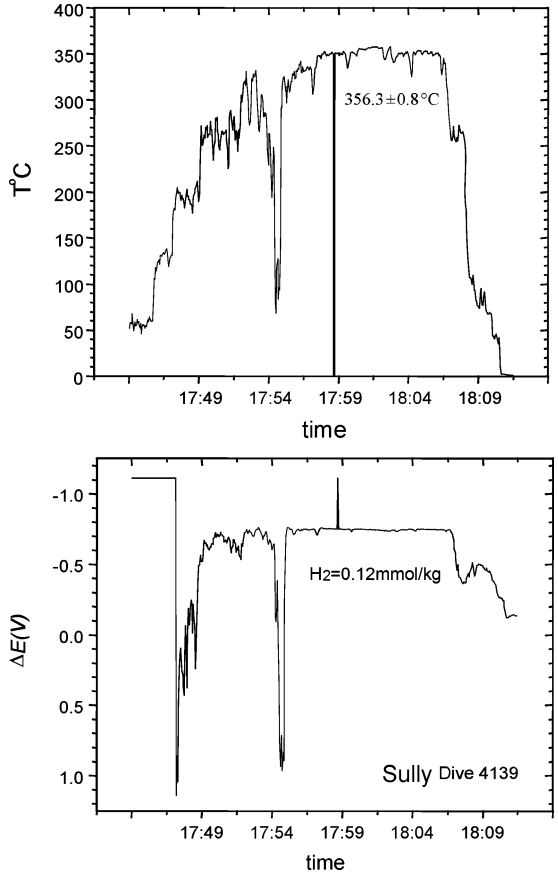

Figure 22. Chemical and temperature data from real-time deployment of the sensor system at Sully vent site (MEF) (modified after ref 79). Measured dissolved H_2 sensor potentials ($\Delta E(V)$) of hydrothermal fluids demonstrate rapid response rate. The time scale is in the format of hour/minute. Changes in temperature indicate seawater-mixing effects. In spite of the dynamic nature of hydrothermal vents, the sensor response is sufficiently rapid to delineate primary (endmember hydrothermal fluids) and secondary (seawater) sources.

The H_2 sensor also performed well when subjected to the more challenging vent environment of the black smoker, where the narrow and irregularly shaped orifice contrasts sharply with measurements performed in the more quiescent flange pools as reviewed above. Clearly, measurements at vent chimney structures enhance the possibility for seawater mixing with attendant effects on temperature and compositional stability. As indicated by H_2 sensor measurements at the Sully black smoker at the Main Endeavour Field (JDF), steady-state chemical and temperature data were still forthcoming (Figure 22).[61]

4.3.2. Steady-State Measurements

Following attainment of steady-state temperature and sensor Emf data, the hydrogen fugacity ($\times c4_{H_2}$) can be determined, which in turn can be used to constrain the dissolved concentration of hydrogen (m_{H_2}) in vent or flange fluids when explicit account is taken of the Henry's law constant for H_2 at conditions equivalent to sensor measurements (eqs 12−14). On the basis of replicate measurements at a wide range of vent and flange sites, the inherent uncertainties in temperature and sensor data are on the order of ±2 °C and ±0.003 V, respectively. The activity of dissolved H_2 determined from sensor data can be compared with data from pressurized fluid samples simultaneously taken from vent/flange sites.[10,12,94] Subsequent shipboard analysis using GC techniques provides a frame of reference against which the in situ dissolved H_2 measurements can be assessed. Comparisons of this sort have been now been carried out during two separate field investigations in 1999 and 2005 to vent/flange sites at the Main Endeavour Field (MEF), Juan de Fuca Ridge.[61,95]

Data obtained at MEF in September 1999 were fortuitously timed, since just 3 months earlier a large seismic event was recorded, located in the immediate vicinity of the Main Endeavour Field. Although the seismic event was interpreted initially as being of tectonic origin,[96] the relatively large increase in the abundance of mantle derived helium and CO_2 in MEF vent fluids[97] suggested that the seismicity may have been more likely related to localized melt migration beneath and slightly offset from the MEF vent system.[82,98] Thus, an opportunity presented itself to test the H_2 sensor under conditions dominated by recent magmatic events that likely were associated with unusually reducing conditions as might be expected from the intrusion of abundant fresh basalt/gabbro into a shallow hydrothermal system. Indeed, the sensor measurements revealed unusually high dissolved H_2 concentrations for many of the vents and flange fluids at MEF (Figure 23).[61] Moreover, where comparisons could be made, the sensor data are generally consistent with those retrieved from the gastight samplers, which were triggered in unison with sensor measurements.[97,98] Differences do exist,

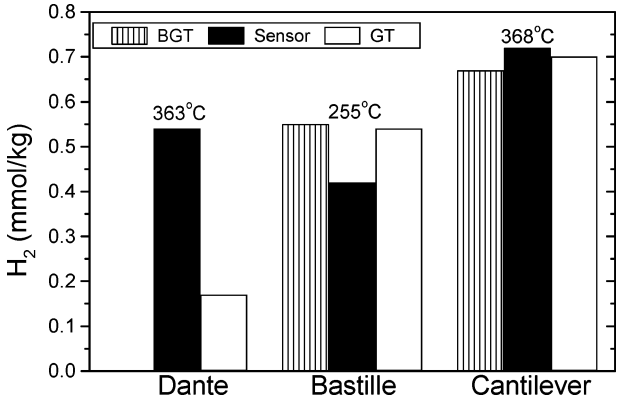

Figure 23. Steady-state concentrations of dissolved H_2 measured for selected hot spring vent fluids and flange pools in the Main Endeavour Field in 1999. Fluid temperatures ranged from approximately 255 to 368 °C, as labeled, which were recorded by the sensor measurements. In general, H_2 concentrations are dominated by temperature and reaction zone characteristics unique to the different vent systems. The figure also provides a comparison of dissolved H_2 concentrations obtained from the in situ sensor and for fluid samples at different vent sites using more conventional approaches. GT, and BGT refer to Gastight Sampler, and Big Gastight sampler (isobaric fluid sampler),[94] respectively. In all of these cases dissolved gases were determined by gas chromatography and the values presented are endmember concentrations (extrapolated to Mg = 0). Vent sites are indicated on *x*-axis. Results show relatively good agreement between the different approaches. The apparent discrepancy for "Dante" may be caused by the relatively low temperature (348 °C) of fluid sampled and measured by the GT sampler in comparison with that measured by the in situ sensor, where the temperature was known to be significantly higher. Reprinted with permission from ref 61. Copyright 2001 from Elsevier.

however, especially for vent fluid at the "Dante" site (Figure 23). Unlike in situ sensor measurements, however, conventional fluid samples taken at this site did not permit simultaneous temperature measurement. Thus, the apparent discrepancy in the case of vent fluids at Dante may result from temperature variability. Dive records in fact reveal a fluid temperature of approximately 348 °C just prior to acquisition of the conventional gas sample at Dante, which is much lower than the temperature recorded by the in situ sensor when deployed. At a seafloor pressure of 220 bar, even slight changes in temperature can cause relatively large changes in dissolved gas concentrations in fluid coexisting with an assemblage of iron oxides and sulfides.[52,63,64,99,100] This, together with the dynamic nature of the vent fluid/seawater environment, where changes in temperature and chemistry are likely, accounts best for the differences between results of the different measurement techniques.

Returning to the MEF hydrothermal vents in August 2005 revealed a dramatically different chemical and physical system. Absent were vent/flange fluids at temperatures in excess of 360 °C. More importantly, virtually all vent fluids in which the in situ chemical sensors were deployed revealed dissolved H_2 concentrations that generally failed to exceed 0.2 mmol/kg.[95] Once again, there was good agreement between chemical sensor data and results from conventional gas-tight samples (Figure 24). The relatively low dissolved H_2 concentrations are likely related to subseafloor hydrothermal alteration processes unperturbed by incipient magmatic injection, as was the case in 1999. Accordingly, more oxidizing conditions prevail in 2005 owing to penetrative alteration of basalt and its alteration products by sulfate-bearing seawater, which stabilizes a secondary mineral

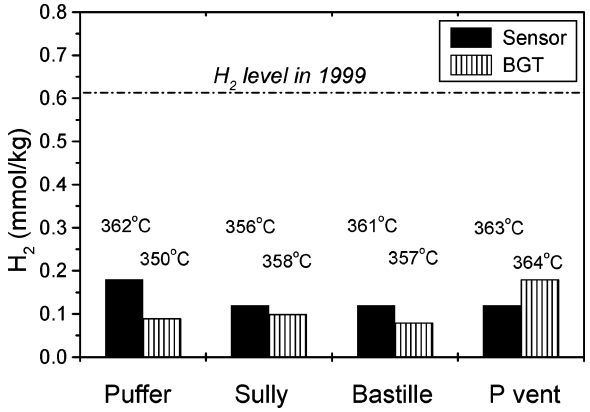

Figure 24. Dissolved H_2 concentrations measured by in situ sensor at MEF (JDF) vents in 2005. Where comparisons can be made, the sensor data agree well with data obtained by more conventional approaches. All of the sensor and sampler data obtained in 2005, however, are considerably lower than those observed in 1999 (indicated with a dashed line,[61] see figure caption and legend in Figure 23), when a subseafloor intrusion of magma significantly perturbed the MEF hydrothermal system. Subsequently, more oxidizing conditions prevail owing to the influx of sulfate-bearing seawater resulting in formation of anhydrite, epidote and other secondary minerals. Similarly oxidizing conditions are reflected by H_2 sensor data obtained at the P-vent site (EPR 9°50′N) in 2004, suggesting common alteration processes and steady-state redox conditions for the two different hydrothermal vent systems.

assemblage characterized by anhydrite−epidote−plagioclase−magnetite ± pyrite.[52,97] In contrast, the relatively high temperatures and highly reducing conditions observed in the immediate aftermath of magmatic/seismic events in 1999 (Figure 23) suggest subseafloor phase equilibria involving pyrite−pyrrhotite−magnetite (PPM). Indeed, theoretical modeling calculations indicate that subseafloor hydrothermal reaction zones may evolve from an initially reducing state characterized by the PPM assemblage toward more oxidizing conditions during the waning stages of subseafloor magmatism.[52,99,100] We hypothesize that the shift in redox is caused largely by a consumption of reduced sulfide originally in the fresh basalt with penetration of increasingly greater amounts of seawater-derived sulfate into high-temperature reaction zones. The availability of in situ chemical sensors to measure and monitor time series changes in vent fluid chemistry represents a new tool with which the source of H_2 variability can be better assessed, and ultimately, more accurately understood in terms of subseafloor hydrothermal alteration processes.

4.3.3. Dynamic Scan Mode

An important advantage of the design of the in situ chemical sensor probe developed for real-time measurements of seafloor vent fluids is that it is ideally suited for use with the manipulator on DSRV *ALVIN* to permit systematic repositioning of the probe within the venting fluid. Accordingly, the role of seawater mixing and vent fluid cooling on redox reactions within the vent plume can be determined. For example, by gradually moving the sensor through the seawater-mixing zone at the margin of the flange pool at Dante vent site during studies at MEF in 1999, the spatial variability of dissolved gas concentrations and temperature were recorded. In effect, the hot-center (370 °C), cool-outer (150 °C) conditions reveal different degrees of mixing between hot hydrothermal fluid and cold seawater (Figure 25).[61] These data reveal increases in H_2 concentrations with

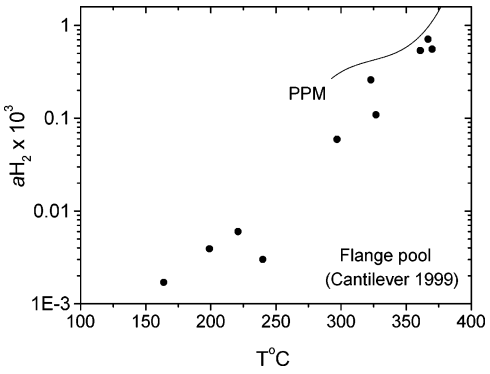

Figure 25. Activities of dissolved H_2 as a function of temperature at seafloor pressure. Results were determined from continuous measurement of fluid in a single flange pool at Cantilever (MEF) with the sensor gradually repositioned to measure fluids at relatively higher and lower temperatures. For comparison, predicted aH_2 in fluid coexisting at equilibrium with pyrite-pyrrhotite-magnetite (PPM) at 300°−370 °C are shown. By using activity terms, the effect of changes in salinity can be eliminated. Our results indicate that dissolved H_2 is at or near PPM levels at the highest temperatures measured, although it decreased with decreasing temperature. Reprinted with permission from ref 61. Copyright 2001 from Elsevier.

increasing temperature. Indeed, the high-temperature data are in excellent agreement with a theoretical projection of H_2 activity with temperature for the assemblage pyrite−pyrrhotite−magnetite, lending support to our previous interpretation of the nature of phase equilibria controls in subseafloor reaction zones at Endeavour. Perhaps more importantly, however, is that with cooling (seawater mixing), H_2 concentrations decrease relative to values predicted for PPM−fluid equilibria. These data are very different from what would be predicted for simple conductive cooling in a closed system, where it can be shown from experimental and theoretical data that H_2 should actually increase.[52] The difference, of course, is entirely related to thermodynamic and kinetic phenomena associated with seawater mixing reactions, which are largely nonconservative processes. That dissolved H_2 concentrations are reduced at 300 °C by approximately 90%, however, indicates the involvement of still other phenomena, which may require consideration of mineral precipitation kinetics. Even at temperatures as low as 200 °C, the fluid still transports significant amounts of dissolved H_2, which may be very significant in terms of energy sources for microbial ecosystems at mid-ocean ridges.[86−90]

4.3.4. Time Series Monitoring

To meet the need for long-term monitoring of vent fluid chemistry, a chemical sensor system that includes a data-logger and on-board operating system, which controls data storage and acquisition rate has been developed.[101,102] The data-logger is contained in a pressure housing and tethered to the sensor (Figure 26). Owing to relatively long-term operational requirements, the gold−H_2 electrode is used with YSZ sensor, which serves as a reference for dissolved H_2 measurement. The gold−YSZ cell design is especially well suited for long-term operation in highly corrosive fluids at elevated temperatures and pressures, as outlined earlier. The preliminary monitoring test was conducted with deployment of the sensor-logger system for a total duration of up to 2 days at "P-vent", EPR 9°N during a cruise to that area in February 2004 (Figure 27). In general, the temperature of

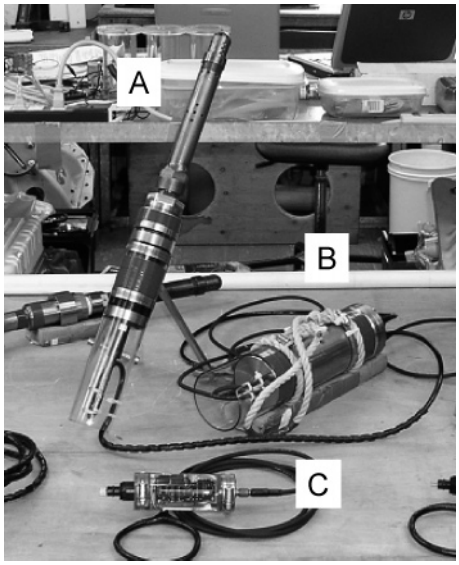

Figure 26. The in situ chemical sensor unit (A) with associated autonomous data logging system (B) for monitoring temperature and chemistry of hydrothermal fluids at seafloor vent sites. Data transfer during the deployment from the submersible is done through a device of ICL communication (C).

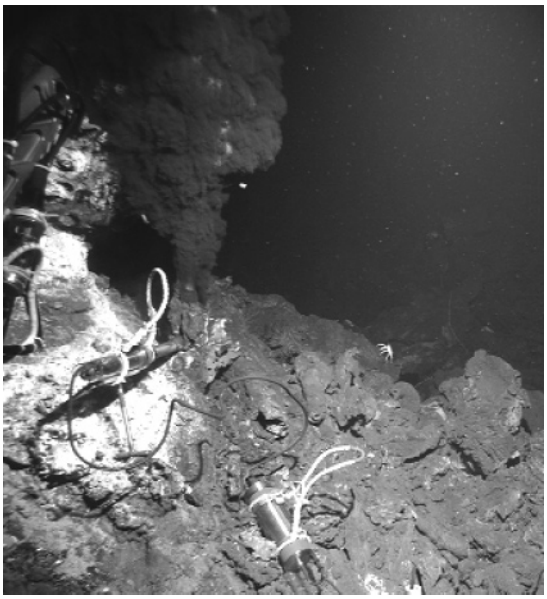

Figure 27. Seafloor deployment of an in situ chemical sensor unit for time series monitoring studies. Preliminary testing was carried out at P-vent (EPR 9°50′N) in 2004.

the vent fluids during sensor deployment was approximately 363−369 °C (Figure 28). The steady-state sensor data yielded values of dissolved H_2 concentration very close to analogous data measured separately at the same vent but at an early time during the same 25-day cruise, using a submersible mounted sensor unit, which provided data output in real-time (Figure 29). As shown in Figure 27, however, chimney construction around the sensor probe deployed continuously for approximately 2 days inhibited seawater mixing, permitting temperatures higher than observed during real-time measurements at the same vent. The higher temperatures were also associated with slightly higher dissolved H_2. Taking account of the temperature variability from one deployment time to the other, the consistency in dissolved H_2, using two different H_2 sensor units is clear. This underscores the reliability of the measurements, especially

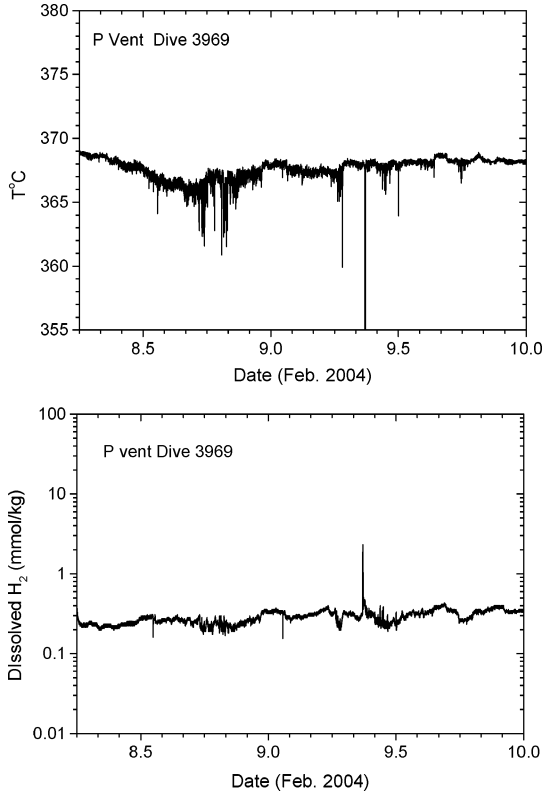

Figure 28. Temperature and dissolved H_2 concentrations recorded during 2-day time-series deployment of the in situ chemical sensor unit in high-temperature hydrothermal fluid issuing from P-vent (EPR 9°50′N). The horizontal time axis is represented by the real GMT date. The minor tick on time axis is therefore in 2 h interval.

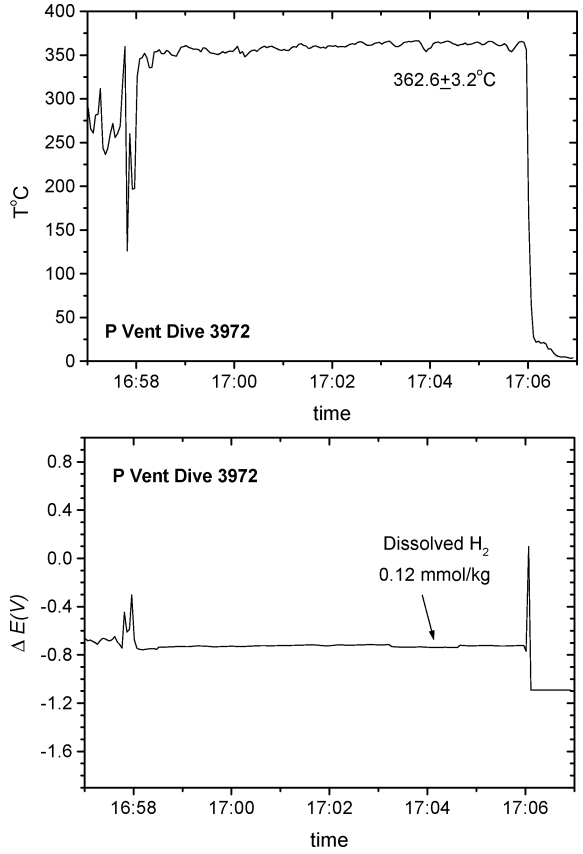

Figure 29. In situ chemical sensor measurement of dissolved H_2 along with fluid temperature at P vent in 2004 (EPR 9°50′N). This particular deployment was conducted in real time mode, independently from the time series monitoring effort depicted in Figure 28. In situ dissolved H_2 concentration determined from the real-time deployment is consistent with data obtained separately from a gastight sample (0.18 mmol/kg, shown in Figure 24), and is also consistent with the value acquired through time series monitoring study (see text and Figure 28). The time axis is in the GMT time with a format of hour/minute.

considering the agreement obtained between these data and analogous data from gas-tight fluid samples taken simultaneously with sensor deployments (Figure 24). The results from seafloor sensor deployments are also in good agreement with results from lab verification studies at similar temperatures, pressures and dissolved H_2 concentrations, providing an additional constraint on the viability of the approach for even longer seafloor deployments. This conclusion is further supported by results from examination of the sensor head following the 2-day vent fluid monitoring study. In general, the electrochemical sensor and coexisting thermocouples were determined to be in excellent condition and required virtually no servicing prior to additional seafloor deployments (Figure 30).

5. Future Prospects

There is no question that pH and dissolved H_2 (redox) represent two of the most critical chemical parameters needed to better understand the chemical and physical evolution of seafloor hydrothermal systems at mid-ocean ridges. Substantial advances have taken place involving the development of high temperature in situ pH and dissolved H_2 sensors, which now permit time series measurements of hydrothermal vent fluids under extreme conditions. Preliminary results from continuous deployment at vents for time periods of days have been very encouraging and well justify even longer deployments (several months) in keeping with the rapidly developing plans for seafloor hydrothermal observatories. The reality of longer-term deployments beyond a time series of several months, however, brings into question a whole series of challenges involving signal integrity and material

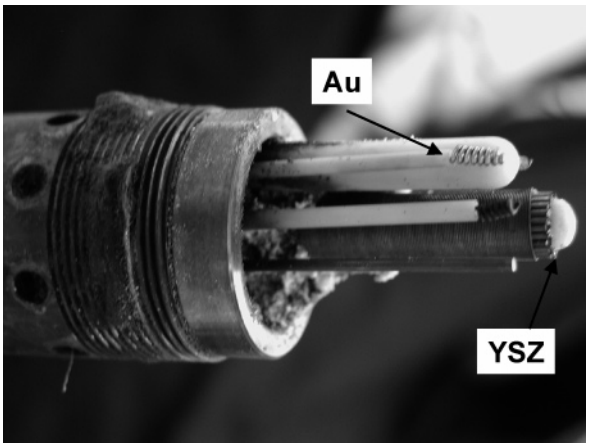

Figure 30. Close-up examination of the electrochemical and thermocouple array following deployment in vent fluid issuing from P-vent at temperatures in excess of 360 °C (EPR 9°50′N). In situ sensors used for dissolved H_2 (Au electrode) and pH (YSZ pH) are appropriately indicated.

properties concerns. Although materials such as zirconia ceramic and gold are well-known for their chemical and thermal resistance, studies are needed to confirm the limited solubility and recrystallization of these materials if longer-term deployment applications are to be realized.

5.1. Long-Term Stability of YSZ Ceramic in Hydrothermal Fluids

As emphasized throughout, the chemical and physical properties of YSZ ceramic play a fundamental role in the performance and application of both pH and dissolved H_2 in situ sensors. Extensive studies were conducted to link the compositional quality of the YSZ ceramic to the sensor performance under hydrothermal conditions.[33,103−107] Experimental results demonstrated that the existence of intergranular oxide and silicate glass in YSZ ceramic decrease its chemical stability.[33,106] It is also noted that high redox-active impurities in YSZ ceramic, such as Fe and Ti ions, may cause mixed conductivity during measurement by the sensor.[104,107] However, the knowledge regarding solubility of the yttria-zirconia solid solution in NaCl-bearing hydrothermal fluid is still lacking.

To further extend our knowledge of the chemical stability of YSZ ceramic in hydrothermal fluids, we have performed a series of experiments at elevated temperatures and pressures applicable to the seafloor hydrothermal vent systems. In addition to the extreme physical conditions, these experiments involved unusually acidic fluids while also having high dissolved chloride concentrations. Accordingly, the combination of chemical and physical conditions go well beyond the limits likely in subseafloor hypothermal fluids, where the in situ pH is buffered at values only slightly acid of neutrality.[7,8,52,81] For comparison, the quench pH equivalent ($pH_{25°C}$) of the slightly acidic condition at elevated temperatures and pressure, is above 3,[8] so pH $_{(25°C)}$ values more acidic than this are unlikely to be encountered in hydrothermal systems at mid-ocean ridges, although such acidic fluids are still useful as a means of testing constraints imposed by pH on the stability of YSZ ceramic.

The YSZ solubility experiments were performed in the previously described titanium flow reactor (Table 1). The Cl-bearing source fluid was acidified so that the fluid pH ($pH_{(25°C)}$) ranged from 1.94 to 4.60. The YSZ ceramic in the reactor at constant temperature and pressure (400 °C, 400 bar) was not in powder form but actually simulated the geometry of an actual sensor used for seafloor trails. The fluid leaving the reactor was then analyzed for a wide range of chemical species. Data reveal low levels of the corrosion. For example, at $pH_{(25°C)}$ of 2.96 and dissolved chloride of 0.55 mol/kg, dissolved Zr and Y indicate low concentrations of 0.05 and 0.24 μmol/kg, respectively, underscoring the limited solubility of these species, which is obviously critical to the functionality of YSZ-based sensor technology.[33] Upon closer inspection of these data, however, it is clear that the dissolved Y/Zr ratio is closely related to fluid pH (Figure 31). At distinctly low pH $_{(25°C)}$ values the solubility of Y exceeds that of Zr, resulting in a high Y/Zr ratio and hinting at incongruent corrosion of YSZ ceramic under these unusually acidic conditions (Figure 31). As emphasized earlier, however, pH $_{(25°C)}$ less than 3 would indicate in situ pH values well below 5,[8] which likely can be ruled out by phase relations in subseafloor reaction zones.[7] At in situ pH values more in keeping with experimental and theoretical data for seafloor hydrothermal vent fluids, Y/Zr concentration ratios are clearly much lower (∼0.2 to ∼4). Although this range of Y/Zr ratio values is not sufficiently high to pose an alarming threat to YSZ sensor applications, concern is still justified, especially considering plans for longer-term deployment scenarios. Accordingly, experimental data are needed to constrain better the implications of sensor-derived Y/Zr ratio levels in fluids on the long-term performance of the YSZ sensor.

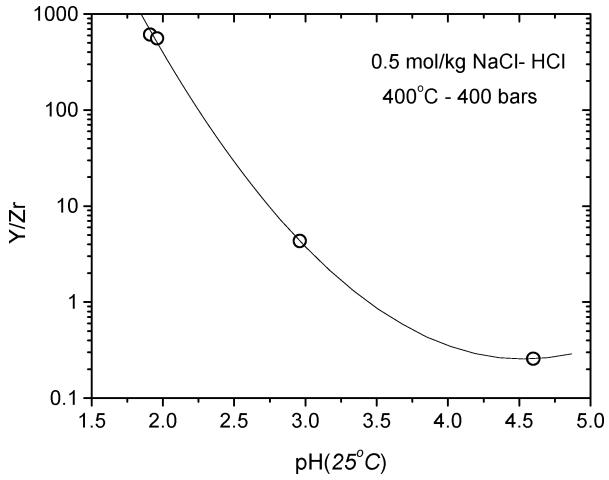

Figure 31. Y/Zr ratio of YSZ ceramic during reaction in the system of NaCl−HCl at 400 °C and 400 bar. Data show an increase in Y/Zr with shapely decreasing pH at experimental conditions. The only slightly acidic conditions typical of subseafloor hydrothermal vent fluids suggest the likelihood of long-term stability of the electrochemical properties of the YSZ sensor.

5.2. Reference Electrode for pH Measurement

Potentially, the most challenging factor related to achieving accurate and long-term in situ pH values of aqueous fluids at elevated temperatures and pressure is not related to the inherent stability of the YSZ−pH sensor, but rather it is the reliability and long-term performance of the coexisting Ag/AgCl electrode, which serves as the reference for in situ pH measurements. Although the Ag/AgCl reference electrode has been calibrated and used with great effect in Cl-bearing hydrothermal fluids,[32,34,108,109] the electrode stability could become unreliable during long-term deployments owing to the potential dissolution of the AgCl component or by sulfidation of Ag.[73,110−112] Thus, research into the chemical and physical stability alternative reference electrodes is necessarily a high priority to more confidently develop long-term deployment strategies involving in situ monitoring of the pH of hydrothermal vent fluids at mid-ocean ridges.

In recent years, there has, in fact, been a good deal of effort dedicated to development of a more reliable reference electrode for use with high temperature aqueous fluids. These efforts, however, have largely been focused on laboratory or industrial applications.[15,16,] One of the effective approaches is to place the reference electrode external to the high-temperature region (EPBRE) to avoid the complications mentioned above.[27,28,113] The main challenge in use of EPBRE method, however, lies to an increased measurement error induced by the thermal liquid-junction potential.[112,114] The recent improvement of EPBRE has effectively addressed this problem by using a flow-through technique with the reference electrode at temperatures up to 400 °C.[33,115] However, due to the need for additional high-pressure pumping system with the reference electrode, this method may not suitable for the application at the seafloor vent system.

Alternative choices for seafloor hydrothermal systems are still very limited. Owing to constraints imposed by seawater composition, Na^+ may be a suitable candidate for use as a component for an alternative reference electrode. In this

regard, we have explored a NASICON based ceramic material, which responds to dissolved Na^+ in aqueous fluids. NASICON, an acronym for Na superionic conductor, is a solid solution in the $NaZr_2(PO_4)_3-Na_4Zr_2(SiO_4)_3$ system with three-dimensional channels that account for the unusual ionic conduction properties of this material.[116] In comparison with YSZ ceramic, the ionic conductivity of NASICON is at least 5 orders of magnitude greater at temperatures of 400 °C.[117] The high conductivity of NASICON enables it to be used as Na^+ sensing material at a range of conditions applicable to seafloor hydrothermal systems. To enhance the corrosion resistance at high-temperature conditions, however, we have eliminated the SiO_4^{4+} component and overexpressed the end member NZP ($NaZr_2(PO_4)_3$ component. For verifying the Na^+ conduction of this NASICON material, we have used seawater as an internal Na reference with this compositional form of the NASICON tube, as illustrated in Figure 32B.

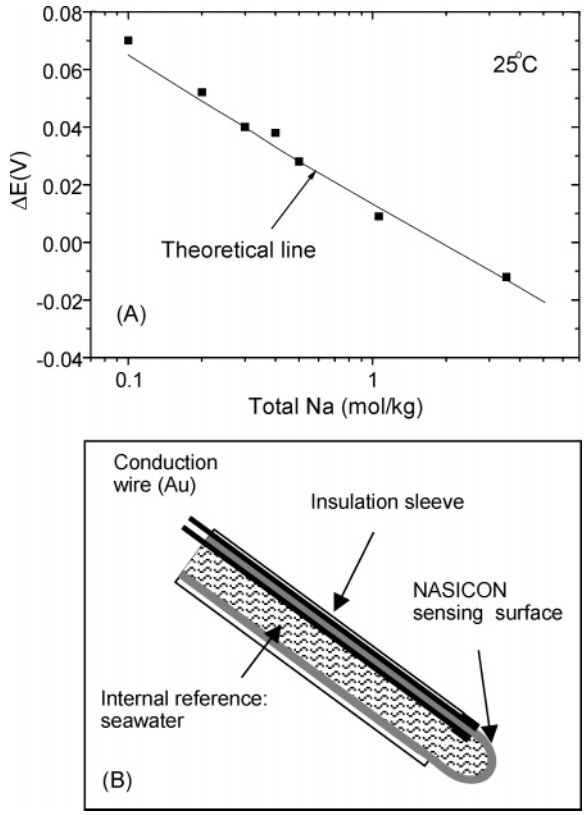

Figure 32. NASICON Na sensor constructed using seawater as internal reference was tested for its Na^+ conduction at room condition. Measured potential $\Delta E(V)$ as a function of total Na concentration is plotted in (A), while the design is shown in (B). Experimental data (solid square) can be compared to theoretical line calculated from eq 17.

Thus, the activity of Na^+ in the test solution (a_{Na+}) can be determined from the measured sensor potential $\Delta E(V)_{Na}$:

$$\log(a_{Na+}) = -\frac{F}{2.303RT}\log(a_{Na+,sw})\Delta E(V) \quad (17)$$

where $a_{Na+,sw}$ is the activity of free Na^+ in seawater at a given temperature and pressure. Preliminary laboratory tests have thus confirmed that NASICON with the previously described composition can serve as a Na^+ sensing material (Figure 32). The key benefit of NASICON technology is far from just making a Na sensor for hydrothermal applications. Indeed, with a proper internal Na^+ sensing element, this material can also be used effectively as a reference electrode for pH determination when linked to the YSZ pH-sensing electrode. Further development is warranted, however, to confirm the performance of the sensor in aqueous fluids at elevated temperatures and pressures, while also constraining the chemical and mechanical stability of the sensor to ensure the long-term reliability needed to meet challenging seafloor applications linked to the proposed ocean observatory initiatives.

6. Conclusions

The highly nonconservative behavior of pH and redox species (H_2, H_2S) during sampling of vent fluid by conventional approaches together with the attendant complications induced by seawater mixing underscores the need for in situ chemical sensors. At present, the availability of in situ sensors that can be used to constrain the chemistry of vent fluids is limited owing to the extreme chemical and physical conditions that characterize these systems. Recently, however, significant progress has been made with chemical sensors utilizing the electrical, mechanical and chemical properties of YSZ ceramic. Experimental and field studies with YSZ-based sensors have documented an unusual degree of chemical and mechanical stability justifying the feasibility of seafloor deployments. When used in combination with the Ag/AgCl reference electrode, the YSZ electrode serves as a pH sensor. The specific ion conducting properties of which enhance transfer of H^+ through the ceramic membrane, which is then recorded by the electrochemical response of an inner reference electrode, usually composed of Hg/HgO. This unique feature of the YSZ sensor precludes the need for calibration, since the electrochemical response is a primary characteristic of the thermodynamic properties of the inner reference. Experimental trials using titanium flow-reactors have confirmed that the YSZ−pH sensor responds rapidly and reversibly to pH at 400 °C and 400 bar. Moreover, these studies have also demonstrated an excellent Nernstian correlation between the measured cell potential and pH calculated at experimental conditions. Verification studies provided by laboratory experiments have justified the design and development of YSZ-based sensor systems that can be used to measure and monitor pH in hydrothermal vent fluids. Successful studies have now been carried out at several hydrothermal vent systems on two different mid-ocean ridges. These data are essential as a means to understand better geochemical controls in subseafloor reaction zones on the evolution of vent fluid chemistry.

Integrating the YSZ-senor with a gold or platinum electrode permits the determination of dissolved H_2 at elevated temperatures and pressures. Experimental and theoretical data confirm that the measured cell potential follows Nernst law predictions for dissolved H_2 concentrations that encompass the full range of values typical of seafloor hydrothermal vent fluids. The Nernstian response not only indicates the viability of the H_2 sensor, but also confirms the thermodynamic basis of the YSZ ceramic membrane electrode, as inferred earlier from in situ pH measurements. As with the YSZ−pH sensor, the YSZ-Au sensor has now been used with great success to both measure and monitor in situ dissolved H_2 concentrations in seafloor hydrothermal fluids at many vent sites. Indeed, real-time measurements of dissolved H_2 using the YSZ-Au sensor have helped to constrain the role of dynamical mixing processes at the vent fluid/seawater interface with corresponding

implications for understanding better a wide range of geochemical and biogeochemical processes on temporal and spatial scales unmatched using other approaches.

Progress in the development and application of in situ sensors for measurement and monitoring of vent fluid chemistry is essential to the realization of many of the goals inherent to a fully functioning seafloor observatory as have been articulated recently by a number of initiatives. Constraints imposed by the extreme chemical and physical conditions that characterize these systems, however, underscore the need to carefully evaluate the chemical and mechanical properties of sensor materials that might be usefully employed for vent fluid chemical monitoring studies. An essential element to accomplish this critical objective, however, involves laboratory testing of signal response characteristics and material properties under the full range of chemical and physical conditions that the senor system will be subjected to on the ocean floor. Thus, laboratory studies at simulated hydrothermal conditions are a necessary step in sensor development if the goals of ocean observatory research at deep-sea vent are to be fully realized.

7. Acknowledgements

We would like to thank Digby D. Macdonald, Naibin Dong, Zhong Zhang, Albert M. Bradley, Canjun Yang, and Ying Chen for their assistance with construction and development of the sensor unit; Jeff Seewald, Dionysis Foustoukos, Michael E. Berndt, Margaret K. Tivey, and Karen L. von Damm are also acknowledged for their help with seafloor deployments and testing of early versions of the chemical sensors developed at the University of Minnesota. We acknowledge the pilots, officers, and crewmembers of Atlantis/Alvin for their dedication and expertise, without which this progress would not have been possible. We would also like to thank Jean Luc Charlou and two anonymous referees for helpful comments and suggestions that contributed substantially to improvement of this paper. Our effort on sensor development was supported by U.S. National Science Foundation Grants EAR-9614427, OCE-9633132, OCE-0117117, and OCE-0525907.

8. References

(1) Edmond, J. M.; Measures, C.; McDuff, R. E.; Chan, L.; Collier, R.; Grant, V.; Gordon, L. I.; Corliss, J. *Earth Planet. Sci. Lett.* **1979**, *46*, 19.
(2) Janecky, D. R.; Seyfried, W. E., Jr. *Geochim. Cosmochim. Acta* **1984**, *48*, 2723.
(3) Bowers, T. S.; Taylor, H. P., Jr. *J. Geophys. Res.* **1986**, *90*, 12583.
(4) Bowers, T. S.; Campbell, A. C.; Measures, C. I.; Spivack, A. J.; Edmond, J. M. *J. Geophys. Res.* **1988**, *93*, 4522.
(5) Campbell, A. C.; Palmer, M. R.; Klinkhammer, G. P.; Bowers, T. S.; Edmond, J. M.; Lawrence, J. R.; Casey, J. F.; Thompson, G.; Humphris, S.; Rona, P.; Karson, J. A. *Nature* **1988**, *335*, 514.
(6) Von Damm, K. L. *Annu. Rev. Earth Planet. Sci.* **1990**, *18*, 173.
(7) Seyfried, W. E., Jr.; Ding, K.; Berndt, M. E. *Geochim. Cosmochim. Acta* **1991**, *55*, 3559.
(8) Ding, K.; Seyfried, W. E., Jr. *Geochim. Cosmochim. Acta* **1992**, *56*, 3681.
(9) Tivey, M. K. In *Seafloor Hydrothermal Systems: Physical, Chemical, Biological, and Geochemical Interactions*; Humphris, S. E.; Zierenberg, R. A.; Mullineaux, L. S.; Thomson, R. E., Eds.; American Geophysical Union: Washington, DC, 1995; p 158.
(10) Von Damm, K. L.; Edmond, J. L.; Grant, B.; Measures, C. I.; Walden, B.; Weiss, R. F. *Geochim. Cosmochim. Acta* **1985**, *49*, 2221.
(11) Butterfield, D. A.; McDuff, R. E.; Mottl, M. J.; Lilley, M. D.; Lupton, J. E.; Massoth, G. J. *J. Geophys. Res.* **1994**, *99*, 9561.
(12) Lilley, M. D.; Butterfield, D. A.; Olson, E. J.; Lupton, J. E.; Macko, S. A.; McDuff, R. E. S. *Nature* **1993**, *364*, 45.
(13) Helgson, H. C.; Kirkham, D. H.; Flowers, G. C. *Am. J. Sci.* **1981**, *281*, 1249.
(14) Bischoff, J. L.; Rosenbauer, R. J. *Earth Planet. Sci. Lett.* **1984**, *68*, 172.
(15) Lvov, S. N.; Palmer, D. A. In *Aqueous Systems at Elevated Temperatures and Pressures: Physical Chemistry in Water, Steam and Hydrothermal Solutions*, Palmer, D. A.; Fernandez-Prini, R.; Harvey, A. H., Eds.; Elsevier Academic Press.: London, 2004; p 377.
(16) Zhu, T.; Guan, X.; Macdonald, D. D. In *Proceedings of Corrosion 2005*; NACE Internal, Houston, TX, 2005; p 05389.
(17) Le Bris, N.; Sarradin, P.; Pennec, S. *Deep-Sea Res. Part I* **2001**, *48*, 1941.
(18) Le Bris, N.; Zbinden, M.; Gaill, F. *Deep-Sea Res. Part I* **2005**, *52*, 1071.
(19) Mesmer, R. E.; Baes, C. F., Jr.; Sweeton, F. H. *J. Phys. Chem.* **1970**, *74*, 1937.
(20) Palmer, D. A.; Hyde, K. E. *Geochim Cosmochim. Acta* **1993**, *57*, 1393.
(21) Benezeth, P.; Palmer, D. A.; Wesolowski, D. J. *Geothermics* **1997**, *26*, 456.
(22) Benezeth, P.; Palmer, D. A.; Wesolowski, D. J. *J. Chem. Eng. Data* **2001**, *46*, 202.
(23) Benezeth, P.; Wesolowski, D. J.; Palmer, D. A. *J. Chem. Eng. Data* **2003**, *48*, 171.
(24) Macdonald, D. D.; Owen, D. *Can. J. Chem.* **1973**, *51*, 2747.
(25) Niedrach, L. W. *J. Electrochem. Soc.* **1980**, *127*, 2122.
(26) Niedrach, L. W. *Science* **1980**, *207*, 1200.
(27) Macdonald, D. D.; Hettiarachchi, S.; Lenhart, S. J. *J. Sol. Chem.* **1988**, *17*, 719.
(28) Hettiarachchi, S.; Makela, K.; Song, H.; Macdonald, D. D. *J. Electrochem. Soc.* **1992**, *139*, L3.
(29) Macdonald, D. D.; Hettiarachchi, S.; Song, H.; Makela, K.; Emerson, R.; Ben-Haim, M. *J. Sol. Chem.* **1992**, *21*, 849.
(30) Ding, K.; Seyfried, W. E., Jr. *Geochim. Cosmochim. Acta* **1995**, *59*, 4769.
(31) Macdonald, D. D.; Kriksunov, L. B. In *Emerging Technologies in Hazardous Waste Management VII* (American Chemical Society Special Symposium Book); Tedder, D. W.; Pohland, F. G., Eds.; Plenum Press: New York, 1995; p 1280.
(32) Ding, K.; Seyfried, W. E., Jr. *Science* **1996**, *272*, 1634.
(33) Lvov, S. N.; Zhou, X. Y.; Ulmer, G. C.; Barnes, H. L.; Macdonald, D. D.; Ulyanov, S. M.; Bening, L. G.; Grandstaff, D. E.; Manna, M.; Vicenzi, E. *Chem. Geol.* **2003**, *198*, 141.
(34) Ding, K.; Seyfried, W. E., Jr.; Tivey, M. K.; Von Damm, K. L.; Bradley, A. M.; Zhang, Z. *Earth Planet. Sci. Lett.* **2005**, *237*, 167.
(35) Niedrach, L. W. *Adv. Ceram. Sci.* **1984**, *12*, 672.
(36) Ding, K.; Seyfried, W. E., Jr. In *Proceedings of the Fifth International Symposium on Hydrothermal Reactions*; Palmer, D. A.; Wesolowski, D. J., Eds.; Oak Rigde National Laboratory: Oak Ridge, TN, 1997; p 145.
(37) Wolery, T. J.; Daveler, S. A. *EQ6, A Computer Program for Reaction Path Modeling of Aqueous Geochemical Systems: Theoretical Manual, Users Guide, and Related Documentation (version 7.0)*; DOE; UCRL-MA-110662 PT IV, 1992.
(38) Bischoff, J. L.; Rosenbauer, R. J. *Geochim. Cosmochim. Acta* **1988**, *52*, 2121.
(39) Shock, E. L.; Helgeson, H. C. *Geochim. Cosmochim. Acta* **1988**, *52*, 2009.
(40) Shock, E. L.; Helgeson, H. C.; Sverjensky, D. A. *Geochim. Cosmochim. Acta* **1989**, *53*, 2157.
(41) Shock, E. L.; Oelkers, E. H.; Johnson, J. W.; Sverjensky, D. A.; Helgeson, H. C. *J. Chem. Soc. Faraday Trans.* **1992**, *88*, 803.
(42) Johnson, J. W.; Oelkers, E. H.; Helgeson, H. C. *Comput. Geosci.* **1992**, *18*, 899.
(43) Ho, P. C.; Palmer, D. A.; Mesmer, R. E. *J. Sol. Chem.* **1994**, *23*, 997.
(44) Sverjensky, A.; Shock, E. L.; Helgeson, H. C. *Geochim. Cosmochim. Acta* **1997**, *61*, 1359.
(45) Ho, P. C.; Palmer, D. A.; Mesmer, R. E. *J. Sol. Chem.* **1994**, *23*, 997.
(46) Ho, P. C.; Palmer, D. A.; Wood, R. H. *J. Phys. Chem. B* **2000**, *104*, 12084.
(47) Ho, P. C.; Palmer, D. A.; Gruszkiewicz, M. S. *J. Phys. Chem. B* **2001**, *105*, 1260.
(48) Hettiarachchi, S.; Kedzierzawski, P.; Macdonald, D. D. *J. Electrochem. Soc.* **1985**, *132*, 1866.
(49) Welhan, J. A.; Craig, H. In *Hydrothermal Processes at Seafloor Spreading Centers*; Rona, P. A., Ed.; Plenum: New York, 1983; p 391.
(50) Merlivat, L.; Pineau, F.; Javoy, M. *Earth Planet. Sci. Lett.* **1987**, *84*, 100.

(51) Seyfried, W. E., Jr.; Ding, K. *Geochim. Cosmochim. Acta* **1993**, *57*, 1905.
(52) Seyfried, W. E., Jr.; Ding, K. In *Seafloor Hydrothermal Systems: Physical, Chemical, Biological, and Geochemical Interactions*; Humphris, S. E.; Zierenberg, R. A.; Mullineaux, L. S.; Thomson, R. E., Eds.; American Geophysical Union: Washington, DC, 1995; p 248.
(53) Chou, I.-M.; Eugster, H. P. *Eos; Trans. Amer. Geophys. Union* **1976**, *57*, 340.
(54) Gunter, W. D.; Myers, J.; Wood, J. R. *Contrib. Mineral. Petrol.* **1979**, *70*, 23.
(55) Gunter, W. D.; Myers, J.; Girsperger, S. In *Hydrothermal Experimental Techniques*; Ulmer, G. C.; Barnes, H. L. Eds.; Wiley-Interscience: New York, 1987; p 100.
(56) Anovitz, L. M.; Blencoe, J. G.; Joyce, D. B.; Horita, J. *Geochim. Cosmochim. Acta* **1998**, *62*, 815.
(57) Frantz, J. In *In-situ Sensors: Their Development and Application for the Study of Chemical, Physical and Biological Systems at Mid-Ocean Ridges*; Seyfried, W. E., Jr.; Johnson, K. S.; Tivey, M. K. Eds.; NSF/RIDGE: Washington DC, 2000; p 6.
(58) Macdonald, D. D.; Mckubre, M. C. H.; Scott, A. C.; Wentrcek, P. R. *Ind. Eng. Chem. Fundam.* **1981**, *20*, 290.
(59) Ding, K.; Seyfried, W. E., Jr. *J. Sol. Chem.* **1996**, *25*, 419.
(60) Eklund, K.; Lvov, S. N.; Macdonald, D. D. *J. Electroanal. Chem.* **1997**, *437*, 99.
(61) Ding, K.; Seyfried, W. E., Jr.; Tivey, M. K.; Bradley, A. M. *Earth Planet. Sci. Lett.* **2001**, *186*, 417.
(62) Kishima, N.; Sakai, H. *Geochem. J.* **1984**, *18*, 19.
(63) Kishima, N. *Geochim. Cosmochim. Acta* **1989**, *53*, 2143.
(64) Ding, K.; Seyfried, W. E., Jr. *EOS; Trans. Amer. Geophys. Union* **1990**, *71*, 1680.
(65) Shock, E. L.; Helgeson, H. C.; Sverjensky, D. A. *Geochim. Cosmochim. Acta* **1989**, *53*, 2157.
(66) Naumov, G. B.; Ryzhenko, B. N.; Khodakovsky, I. L. *Handbook of Thermodynamic Data;* USGS(WRD-74-001.): Washington, DC, 1974.
(67) Haar, L.; Gallagher, J.; Kell, G. *NBS/NRC Steam Tables*; Hemisphere Publishing Corporation, 1984.
(68) Robie, R. A.; Hemingway, B. S.; Fisher, J. R. *U.S. Geol. Surv. Bull.* **1978**, *1452*.
(69) Clemens, J. D.; McKibben, M. A. In *Hydrothermal Experimental Techniques*, 2nd ed.; Ulmer, G. C.; Barnes, H. L., Eds.; Wiley-Interscience: New York, 1987; p 138.
(70) Oudar, J. *Catal. Rev. Sci. Eng.* **1980**, *22*, 171.
(71) Hegedus, L.; McCabe, R. W. *Catal. Rev. Sci. Eng.* **1981**, *23*, 377.
(72) Chou, I-M. *Am. J. Sci.* **1986**, *286*, 638.
(73) Hills, G. J.; Ives, D. J. G. In *Reference Electrodes: Theory and Practice*; Ives, D. J. G.; Janz, G. J. Eds.; Academic Press: New York, 1961; p 73.
(74) Hammer, B.; Norskov, J. K. *Nature* **1995**, *376*, 238.
(75) Weewer, R.; Hemmes, K.; de Wit, J. H. W. *J. Electrochem. Soc.* **1995**, *142*, 389.
(76) Seyfried, W. E., Jr.; Janecky, D. R.; Berndt, M. E. In *Hydrothermal Experimental Techniques*, 2nd ed.; Barnes, H. L.; Ulmer, G. C., Eds.; Wiley Intercience: New York, 1987; p 216.
(77) Seyfried, W. E., Jr.; Ding, K. *Geochim. Cosmochim. Acta* **1993**, *57*, 1905.
(78) Ding, K.; Seyfried, W. E., Jr.; Bradley, A. M.; Tivey, M. K. *EOS; Trans. Amer. Geophys. Union* **1998**, *79*, F67.
(79) Ding, K; Zhang, Z.; Seyfried, W. E. Jr.; Bradley, A. M.; Zhou, Y.; Yang, C.; Chen, Y. In *Proceedings of OCEAN'06 MTS/IEEE-Boston*, 2006; p 060331-159.
(80) Bradley, A. M.; Tivey, M. K.; Liberatore, S. P.; Duester, A. R. *EOS; Trans. Amer. Geophys. Union* **1995**, *71*, 411.
(81) Barnes, H. L. In *Geochemistry of hydrothermal ore deposits*; Barnes, H. L., Ed.; Wiley: New York, 1979; p 404.
(82) Seyfried, W. E., Jr.; Seewald, J. S.; Berndt, M. E.; Ding, K.; Foustoukos, D. *J. Geophys. Res.* **2003**, *108*, 2429.
(83) Ding, K.; Seyfried, W. E., Jr. *Mineral. Mag.* **1994**, *58A*, 231.
(84) Baker, E. T.; Massoth, G. J.; de Ronde, C. E. J.; Lupton, J. E.; McInnes, B. I. *Geology* **2002**, *30*, 975.
(85) Tivey, M. K. Humphris, S. E.; Thompson, G.; Hannington, M.; Rona, P. A. *J. Geophys. Res.* **1995**, *100*, 12527.
(86) Reysenbach, A. L.; Shock, E. *Science* **2002**, *296*, 1077.
(87) Alain, K.; Zbinden, M.; Le Bris, N.; Lesongeur, F.; Querellou, J.; Gaill, F.; Cambon-Bonavita, M.-A. *Environ. Microbiol.* **2004**, *6*, 227.
(88) Page, A.; Juniper, S. K.; Olagnon, M.; Alain, K.; Desrosiers, G.; Querellou, J.; Cambon-Bonavita, M. A. *Geobiol.* **2004**, *2*, 225.
(89) Lloyd, K. G.; Edgcomb, V. P.; Molyneaux, S. J.; Böer, S.; Wirsen, C. O.; Atkins, M. S.; Teske, A. *Appl. Environ. Microbiol.* **2005**, *71*, 6383.
(90) Schrenk, M. O.; Kelley, D. S.; Delaney, J. R.; Baross, J. A. *Appl. Environ. Microbiol.* **2003**, *69*, 3580.
(91) Seewald, J. S.; Seyfried, W. E., Jr. *Earth Planet. Sci. Lett.* **1990**, *101*, 388.
(92) Seyfried, W. E., Jr.; Ding, K.; Berndt, M. E.; Chen, X. *Rev. Econ. Geol.* **1999**, *8*, 181.
(93) Charlou, J. L.; Fouquet, Y.; Donval, J. -P.; Auzende, J. -M.; Jean-Baptiste, P.; Stievenard, M.; Michel, S. *J. Geophys. Res.* **1996**, *101*, 15,899.
(94) Seewald, J. S.; Doherty, K. W.; Hammar, T. R.; Liberatore, S. R. *Deep Sea Res. Part I* **2002**, *49*, 189.
(95) Ding, K.; Seyfried, W. E., Jr.; Zhang, Z.; Foustoukos, D.; Pester, N. J. *EOS, Trans. Am. Geophy. Union* **2005**, *86*, T31A-0488.
(96) Johnson, H. P.; Hutnak, M.; Dziak, R. P.; Fox, C. G.; Urcuyo, I.; Cowen, J. P.; Nabelek, J. L.; Fisher, C. R. *Nature* **2000**, *407*, 174.
(97) Lilley, M. D.; Lupton, J. E.; Butterfield, D. A.; Olson, E. *Nature* **2003**, *422*, 878.
(98) Seewald, J.; Cruse, A. M.; Saccocia, P. J. *Earth Planet. Sci. Lett.* **2003**, *216*, 575.
(99) Ding, K.; Seyfried, W. E., Jr. *EOS; Trans. Amer. Geophys. Union* **1993**, *74*, 323.
(100) Seyfried, W. E., Jr.; Ding, K.; Rao, B. In *Water-Rock Interactions, Ore Deposits, and Environmental Geochemistry*; Hellmann, R.; Wood, S. A., Eds.; The Geochemical Society: St. Louis, MO, 2002; p 257.
(101) Ding, K.; Seyfried, W. E., Jr.; Zhang, Z.; Yang, C.; Foustoukos, D. *Eos, Trans. Am. Geophys. Union* **2004**, *85*, B131A-0170.
(102) Yang, C.; Chen, Y.; Gu, L.; Ye, Y.; Cao, J.; Ding, K. *EOS Trans. Am. Geophys. Union* **2004**, *85*, OS43B-0554.
(103) Sato, M. In *Research Techniques for High Temp. and High Pressure*; Ulmer, G. C., Ed.; Springer-Verlag: New York, 1971; p 43.
(104) Ulmer, G. C. *Adv. Ceram. Sci.* **1984**, *12*, 660.
(105) Baumard, J. F.; Abelard, P. *Adv. in Ceram.* **1984**, *12*, 555.
(106) Badwal, S. P. S.; Drennan, J. *Int. Phys. Conf. Ser.* **1988**, *89*, 277.
(107) Merino, R. I.; Nicoloso, N.; Maier, J. In *Ceramic Oxygen Ion Conductors and Their Technological Applications*; Steele, B. C. H., Ed.; University Press: Cambridge, UK, 1996; p 43.
(108) Huang, S.; Daehling, K.; Carlston, T. E.; Propp, A. *Corrosion* **1991**, *47*, 185.
(109) Kerner, Z.; Balog, J.; Nagy, G. *Corros. Sci.* **2006**, *48*, 1899.
(110) Greeley, R. S.; Smith, W. T.; Stoughton, R. W.; Lietzke, M. H. *J. Phys. Chem.* **1960**, *64*, 652.
(111) Lietzke, M. H.; Hupf, H. B.; Stoughton, R. W. *J. Phys. Chem.* **1965**, *69*, 2395.
(112) Macdonald, D. D.; Kriksunov, L. B. *Corros.* **1978**, *34*, 75.
(113) Macdonald, D. D.; Scott, A. C.; Wentrcek, P. *J. Electrochem. Soc.* **1979**, *126*, 908.
(114) Lvov, S. N.; Macdonald, D. D. *J. Electroanal. Chem.* **1996**, *403*, 25.
(115) Lvov, S. N.; Zhou, X. Y.; Macdonald, D. D. *J. Electroanal. Chem.* **1999**, *463*, 146.
(116) West, A. R. In *Solid State Electrochemistry*; Bruce, P. G., Ed.; Cambridge University Press: Oxford, 1995; p 7.
(117) Kudo, T. In *The CRC Handbook of Solid State Electrochemistry*; CRC Press: 1997; Boca Raton, FL; p 195.

CR050367S